Lysophosphatidylcholines are elevated after selective serotonin reuptake inhibitor exposure during neural differentiation and correlate with early neurodevelopmental symptoms

Abishek Arora[1,2,3], Kristina Vacy[4,5#], Cátia Marques[6#], Mihai-Ovidiu Degeratu[1,2], Francesca Mastropasqua[1,2], Jenny Humphrey[1,2], Xuan Ye[1,2], Marika Oksanen[1,2], the Barwon Infant Study Investigator Group, Peter Vuillermin[4,7], Anne-Louise Ponsonby[4,7], Ingela Lanekoff[6,8] and Kristiina Tammimies[1,2,*]

[1]Center of Neurodevelopmental Disorders (KIND), Centre for Psychiatry Research, Department of Women's and Children's Health, Karolinska Institutet, and Child and Adolescent Psychiatry, Stockholm Health Care Services, Region Stockholm, Stockholm, Sweden.

[2]Astrid Lindgren Children's Hospital, Karolinska University Hospital, Region Stockholm, Stockholm, Sweden.

[3]SciLifeLab, Department of Women's and Children's Health, Karolinska Institutet, Stockholm, Sweden.

[4]Florey Institute of Neuroscience and Mental Health, University of Melbourne, Victoria, Australia

[5]Melbourne School of Population and Global Health, University of Melbourne, Victoria, Australia.

[6]Department of Chemistry - BMC, Uppsala University, Uppsala, Sweden.

[7]Murdoch Children's Research Institute, Royal Children's Hospital, and Department of Paediatrics, University of Melbourne, Victoria, Australia.

[8]Center of Excellence for the Chemical Mechanisms of Life, Uppsala University, Uppsala, Sweden.

[#]These authors contributed equally to this work

[*]Correspondence: kristiina.tammimies@ki.se

Corresponding author

Kristiina Tammimies, PhD

Postal address: Biomedicum A4, Karolinska Institutet, 171 77 Stockholm, Sweden

E-mail: kristiina.tammimies@ki.se

SUMMARY

Selective serotonin reuptake inhibitors (SSRIs) are often prescribed during pregnancy. Yet, epidemiological studies associate *in-utero* SSRI exposure with neurodevelopmental disorders, such as autism and attention-deficit/hyperactivity disorder (ADHD). The potential molecular mechanisms by which SSRIs impact early neurodevelopment are not fully understood. In this study, we examined the effects of four commonly prescribed SSRIs—fluoxetine, citalopram, sertraline, and paroxetine—on neuroepithelial stem cells derived from four different human induced pluripotent stem cells. Following SSRI exposure, we assessed cellular viability, reactive oxygen species (ROS) levels, mitochondrial function through adenosine triphosphate (ATP) assays and performed high throughput metabolomic profiling at two timepoints: proliferation and neural differentiation stages. Sertraline and paroxetine significantly decreased ROS and ATP levels, indicating mitochondrial alteration. Metabolomic analysis identified several affected pathways and pinpointed three lysophosphatidylcholines (LPCs) 16:0, 18:0, and 18:1 as significantly elevated across all SSRI exposures and time points, except for citalopram. In a complementary population-based cohort study, the Barwon Infant Study (BIS), consisting of 1074 mother-child pairs, we further observed elevated LPC levels in the cord blood of infants prenatally exposed to SSRIs, with a dose-dependent correlation to autism and ADHD-related symptoms at age two. These findings provide insights into SSRI-induced molecular changes, identify potential biomarkers for SSRI exposure monitoring, and emphasize the need for further clinical investigations into prenatal SSRI exposure and neurodevelopmental outcomes.

INTRODUCTION

Selective serotonin reuptake inhibitors (SSRIs) are widely prescribed antidepressants that block the reuptake of serotonin by binding to the serotonin transporter, resulting in elevated levels of serotonin in the synaptic cleft (Hiemke and Härtter, 2000). Depression affects ~28% of pregnant women (Al-abri et al., 2023) and SSRI use during pregnancy has increased over recent decades (Tran and Robb, 2015). Therefore, it is critical to understand their impact on foetal development. Although considered relatively safe, several epidemiological studies suggest that SSRI exposure during pregnancy may increase the likelihood of neurodevelopmental disorders (NDDs), including autism and attention-deficit/hyperactivity disorder (ADHD). For instance, a meta-analysis of 18 studies showed that *in-utero* exposure to SSRIs increases the likelihood of autism (hazard ratio, HR=1.27; 95% confidence interval, CI=1.10–1.47) (Halvorsen et al., 2019). Nevertheless, several confounding factors, including

shared genetic liability factors, could still influence this. Beyond NDDs, a recent review has found a strong association of different SSRIs with several adverse foetal health outcomes (Desaunay et al., 2023), including an increased burden of cardiovascular complications in neonates (De Vries et al., 2021; Knudsen et al., 2014).

Sertraline, citalopram, paroxetine, and fluoxetine are the most commonly prescribed SSRIs to women of reproductive age (Anderson et al., 2020; Dawson et al., 2016). These SSRIs vary in properties such as half-life (approximately 21 hours to a few days), the relationship between dose/blood levels and the dose range of prescription (Marken, 2000). SSRIs can cross the placenta (Hendrick et al., 2003) and subsequently alter foetal serum serotonin levels (Anderson et al., 2004), with a plausible impact on the developing brain (Olivier et al., 2013). Neurodevelopment at the early stages of gestation, prior to the formation of the intact blood-brain barrier (Risau and Wolburg, 1990) and widespread synaptic connectivity, relies on regulation by neurotransmitters (Rock and Patisaul, 2018). Serotonergic activity is one of the building blocks of neuronal organisation, with serotonin being one of the first neurotransmitters to emerge (Brummelte et al., 2017).

Although many uncertainties remain around SSRIs and their mechanism of action, few studies have demonstrated wide-ranging cellular effects, including an alteration in reactive oxygen species (ROS) levels (Behr et al., 2012) and an impact on mitochondrial oxidative phosphorylation (Emmerzaal et al., 2021). During neurodevelopment, ROS functions as a signalling molecule contributing to neuronal growth and synaptogenesis (Oswald et al., 2018). However, excessive ROS-induced oxidative stress can lead to genetic mutations, lipid peroxidation, and mitochondrial dysfunction (Wang, 2010). Furthermore, in a previous study, we have demonstrated that fluoxetine exposure alters lipid and energy metabolism, observed in both the transcriptome and metabolome of differentiating neuroepithelial stem (NES) cells (Arora et al., 2023). Despite these efforts, there are no systematic studies investigating the potential molecular mechanisms of SSRI exposure in early neuronal development and how these could link to NDDs.

In this study, we used human induced pluripotent stem cell (iPSC)- derived NES cells undergoing undirected differentiation into neurons and exposed them to four commonly prescribed SSRIs. First, we evaluated the effects of SSRI exposure on cellular viability, ROS, and oxidative phosphorylation of ATP. After establishing these *in-vitro* effects, we performed untargeted mass spectrometry analysis to develop metabolomic profiles of the general and specific effects of each SSRI.

We then analysed the top three upregulated lipids from the cellular models in cord blood from a population-based cohort, the Barwon Infant Study (BIS), consisting of 1074 mother-child dyads, and investigated the association between SSRI exposure, the cord blood lipid levels and correlation with autism and ADHD traits at age two.

We provide evidence of dysregulated cellular and lipid profiles of differentiating neural cells after SSRI exposure and validate the most upregulated and consistent lipids in a population-based cohort. Our comprehensive translational study can lead to recommendations for future epidemiological and clinical evaluations on understanding the effects of SSRIs during pregnancy and neurodevelopment.

RESULTS

Increased comparative cytotoxicity is observed with sertraline

We studied the *in-vitro* effects of four SSRIs, namely fluoxetine hydrochloride (FH), citalopram hydrobromide (CH), sertraline hydrochloride (SH) and paroxetine hydrochloride (PH) using four human iPSC derived NES cell lines, of which two were from individuals with NDDs and known pathogenic genetic variants (Becker et al., 2020; Falk et al., 2012; Mastropasqua et al., 2022; Uhlin et al., 2017). NES cells underwent undirected differentiation for up to 28 days, with and without SSRI exposure.

First, we tested the optimal concentrations for SH, CH, and PH using the $CTRL_{Male}$ cell line, similar to our prior work with FH (Arora et al., 2023). Using an exposure range between 0.0–30.0 µM, cell viability was assessed using the MTS assay at 24- and 120-hours post-differentiation. The highest concentration with no significant reduction in viability (Tukey post hoc $p>0.05$) or observable changes in cellular morphology under phase-contrast microscopy at day 5 was selected. Based on these criteria, the optimal concentrations were 3.0 µM for FH, CH, and PH and 1.5 µM for SH (Figure S1A). SH demonstrated increased cytotoxicity at 120 hours post-differentiation compared to the other SSRIs, for which its optimal concentration was adjusted.

Sertraline and paroxetine decrease cellular ROS and ATP levels

Total ROS levels were detected using the DCFDA (2',7'-dichlorodihydrofluorescein diacetate) assay at day 5 and 28 of differentiation in the four cell lines. At day 5 and day 28, a significant (Nemenyi post hoc $p=0.005$) reduction in ROS levels was detected for SH exposure (Figure 1A). For PH, significantly reduced total ROS levels were detected at day 28 (Nemenyi post hoc $p=0.007$) (Figure 1A).

To correct for the Crabtree Effect, where cells in culture prefer glycolysis over oxidative phosphorylation (Mot et al., 2016), the cells were assayed in a cell medium in which glucose was replaced with galactose to promote ATP generation by oxidative phosphorylation (Figure S1B). CH significantly increased (Tukey post hoc p=0.0004) total ATP levels, while PH caused a decrease (Tukey post hoc p<0.0001) at day 5 (Figure 1B). At day 28, no difference was observed with CH compared to the control; however, both SH (Holm adj. p<0.0001) and PH (Holm adj. p=0.005) decreased total ATP levels (Figure 1B).

Early metabolic changes are induced by sertraline

Mass spectrometry-based untargeted metabolomics revealed over 2500 metabolite signals, including adducts, in our cell lysates. Of these, 189 unique metabolites met the signal threshold and were quantified at both day 5 and day 28 post neural differentiation and SSRI exposure. At day 5, cells were exposed to FH, CH, and PH at 3.0 µM and SH at 1.5 µM, and the exposure was validated in the metabolomics data (Figure S1C). Principal component analysis (PCA) revealed overlapping metabolic profiles across the SSRI treatments, with PC1 and PC2 accounting for 43.5% of the total variability (32.6% and 10.9%, respectively) (Figure S2A).

Using a mixed linear model accounting for the genetic background and the exposure followed with FDR correction, we report that SH modulated the largest number of metabolites (52 metabolites), followed by PH (19 metabolites), FH (9 metabolites), and CH (1 metabolite) at day 5 (Table S1A). For SH, the metabolites spanned seven classes: acylcarnitines, amino acids, lysophospholipids, phosphatidylcholines, phosphatidylethanolamines, plasmanylcholines and sugars (Figure 1C). Amino acids such as glutamic acid (SH, adj. p=0.001; PH, adj. p=0.019), methionine (SH, adj. p=0.004; PH, adj. p=0.027), threonine (SH, adj. p=0.001; PH, adj. p=0.014), and lysine (SH, adj. p=0.004; PH, adj. p=0.049) were reduced by both SH and PH (Figure 1D). Feature selection analysis of day 5 data highlighted ten significant metabolites across SSRI treatments (Table S1B). The lysophosphatidylcholines – LPC 16:0, LPC 14:0, and LPC 18:0 emerged as the top three features, each with a combined p-value of <0.0001.

Paroxetine and sertraline share metabolic profiles following prolonged exposure

For the day 28 metabolomics analysis, all four cell lines were treated with SSRIs at a standardized concentration of 1.5 µM, based on the SH treatment level. These exposures were

confirmed in the samples (Figure S1C). Again, PCA did not show clear clustering by treatments (Figure S2B). PC1 and PC2 explained 38.1% of the variance (22.8% and 15.3%, respectively).

The mixed linear model analysis detected the highest number of metabolite changes after PH treatment (64 metabolites), followed by SH (61 metabolites), FH (28 metabolites), and CH (1 metabolite) (Table S2A). Most metabolites affected by SH, FH, and CH were also modulated by PH (Figure 1C). For instance, PC 30:0 was significantly reduced by all SSRIs (FH, adj. p=0.004; CH, adj. p=0.040; SH, adj. p=0.018; PH, adj. p=0.0001). Amino acids such as glutamine (FH, adj. p=0.007; SH, adj. p=0.003; PH, adj. p=0.005), proline (FH, adj. p=0.004; SH, adj. p=0.003; PH, adj. p=0.004), and threonine (FH, adj. p=0.002; SH, adj. p=0.001; PH, adj. p=0.001) were decreased across these treatments (Figure 1D). GABA was specifically reduced by SH (adj. p=0.023) and PH (adj. p=0.035) (Figure 1D).

LPCs (18:0, 18:1, 16:0) were consistently elevated: LPC 18:0 (FH, adj. p=0.002; SH, adj. p<0.0001; PH, adj. p<0.0001), LPC 18:1 (FH, adj. p=0.001; SH, adj. p<0.0001; PH, adj. p=0.001), and LPC 16:0 (SH, adj. p<0.0001; PH, adj. p=0.008) (Figure 1D). Feature selection using metabolite data from day 28 identified 24 significant metabolites (Table S2B). The top three features were LPC 18:0 (combined p<0.0001), LPC 18:1 (combined p=0.001), and LPC 16:0 (combined p=0.002).

Phospholipid biosynthesis and amino acid metabolism are key pathways modulated by SSRI exposure

Using metabolite-set enrichment analysis (MSEA) and quantitative enrichment analysis (QEA), significant biochemical pathways affected by SSRI exposures were identified. At day 5, exposure to FH (Figure 2A, Table S3A) resulted in the enrichment of ten pathways, including phospholipid biosynthesis (adj. p=0.0001), galactose metabolism (adj. p=0.0001), and sphingolipid metabolism (adj. p=0.001). SH exposure significantly enriched 48 pathways (Table S3C), notably phospholipid biosynthesis (adj. p<0.0001), purine metabolism (adj. p=0.001), and tryptophan metabolism (adj. p=0.001) (Figure 2A and S2C). Similarly, PH exposure enriched 50 pathways (Table S3D), including phospholipid biosynthesis (adj. p<0.0001), purine metabolism (adj. p=0.014), and tryptophan metabolism (adj. p=0.027) (Figure 2A and S2D). In contrast, CH exposure did not result in significant pathway enrichment (Table S3B).

At day 28, similar results were observed. FH exposure enriched ten pathways (Table S4A), such as galactose metabolism (adj. p=0.0003), sphingolipid metabolism (adj. p=0.003), and phospholipid biosynthesis (adj. p=0.007) (Figure 2A). SH exposure led to the enrichment

of 54 pathways (Table S4C), including phospholipid biosynthesis (adj. p<0.0001), purine metabolism (adj. p=0.0002), and phenylalanine and tyrosine metabolism (adj. p=0.003) (Figure 2A and 2B). PH exposure enriched 46 pathways (Table S4D), including phospholipid biosynthesis (adj. p=0.0001), purine metabolism (adj. p=0.018), and phenylalanine and tyrosine metabolism (adj. p=0.041) (Figure 2A and 2C). CH exposure continued to show no significant pathway enrichment (Table S4B).

These findings emphasize the consistent enrichment of key biochemical pathways, particularly phospholipid biosynthesis and amino acid metabolism, in response to FH, SH, and PH exposures. This highlights the central role of these pathways in SSRI-induced metabolic effects.

Selected LPCs associate with *in-vitro* and *in-vivo* SSRI exposures

As LPC 18:0, LPC 18:1, and LPC 16:0 were the most consistent findings within the cellular exposure metabolic screening at both time points (Figure 1D and 3A), we continued to investigate their effects both *in-vitro* and *in-vivo*. First, we hypothesized that LPCs could contribute to changes in ROS and ATP levels that were observed after the SH and PH exposures (Figure 1A and 1B). To test this, we inhibited LPC production using the phospholipase A2 inhibitor arachidonyl trifluoromethyl ketone ($AACOCF_3$, 10 μM) for 24 hours, as well as treated the cells with a combination of the LPCs (18:0, 18:1, 16:0) and SH. The 24-hour inhibition of the LPC production attenuated the reduction of ROS both at day 5 and day 28 in the SH-treated cells; however, there was no significant difference between the two conditions (Figure 3B). For ATP production, the LPC production inhibition only slightly attenuated the effect of SH on day 5 and seemed to enhance the reduction on day 28 (Figure 3C). Interestingly, the combination of LPCs increased the ROS and ATP levels at both time points (Figure S2E and S2F). We can conclude that the three LPCs and the inhibition of their synthesis cause a change in ROS and ATP levels, but inconsistently, pinpointing to more complex regulatory patterns.

Next, we used metabolic and neurodevelopmental outcome data from the BIS cohort (Vacy et al., 2024), comprising 1,074 mother-child pairs, to analyse the LPC effects in a population-based cohort. First, we investigated the associations between maternal SSRI use (n=40) and any antidepressant use (n=48) within the first and second trimesters on the levels of the selected LPCs (Figure 3D, Table S5A) in the infant cord blood. Our findings indicate that prenatal SSRI use was associated with elevated levels of cord blood LPC 16:0 sn1 (β=0.173, 95% CI=0.011–0.334; p=0.037), and LPC 16:0 sn2 (β=0.175, 95% CI=0.007–0.343;

p=0.042), and LPC 18:0 sn2 (β=0.174, 95% CI=0.018–0.330; p= 0.029). Additionally, we observed trends (p<0.1) suggesting higher levels of LPC 18:0 sn1 and LPC 18:1 sn2 with prenatal SSRI use. When analysing the effects of any antidepressant use, which added eight additional mothers on other antidepressants, these associations were attenuated (Figure 3D, Table S5A). There were no significant correlations between maternal prenatal Edenborough Depression Scale (EBDS) scores and any of the LPCs studied (Figure 3D, Table S5A). Furthermore, no significant associations were found between prenatal SSRI use and maternal LPC levels at 28 weeks of gestation or with the infant's LPC levels at 6 months, 12 months, and 4 years (data not shown).

We previously published the significant positive associations between the LPCs and ratings using the Child Behavior Check List (CBCL) for autism and ADHD symptom scales, showing significant associations (Vacy et al., 2024). Here, we further examined the relationship between the three consistently upregulated LPCs and the outcomes by categorizing each LPC measure into quartiles. This approach allowed us to explore potential non-linear associations with CBCL-autism and CBCL-ADHD scores and assess dose-response relationships. Significant associations were found for LPC 16:0 sn2 with CBCL-autism scores (overall p=0.01) and for both LPC 16:0 sn1 and LPC 16:0 sn2 with CBCL-ADHD scores (overall p=0.007 and 0.002, respectively) (Figure 3E, Table S5B).

When investigating outcomes older than two years of age, we did not observe significant associations between any of the LPCs and autism/ADHD-related measures from the strength and difficulties questionnaire (SDQ) at age 4 for hyperactivity difficulties, peer problem difficulties, prosocial behaviour strengths, or parent-reported autistic traits (data not shown).

DISCUSSION

We have investigated the effects of four commonly prescribed SSRIs to women of reproductive age on human iPSC-derived neuroepithelial stem cells undergoing undirected differentiation for 5 and 28 days towards neurons using four genetically distinct human iPS cell lines. Exposure to SH and PH, of which the latter is not clinically recommended during pregnancy (Bérard et al., 2016), notably decreased total ROS and ATP levels, implicating mitochondrial dysfunction. The metabolomic analysis further identified multiple significantly modulated metabolites predominantly driven by SH and PH, enriched in energy metabolism and amino acid pathways. Importantly, we identified elevated lysophosphatidylcholines (LPC 16:0, LPC 18:0, and LPC 18:1) as robust molecular signatures consistent across cellular models and

clinical samples, underscoring their potential clinical significance. The clinical validation using the population-based BIS cohort confirmed the LPC 16:0 and LPC 18:0 as potential biomarkers correlating with prenatal SSRI exposure. Our data provides evidence supporting these LPCs as early biomarkers indicating elevated likelihood for early autism and ADHD-related traits, suggesting that altered LPC levels could potentially guide proactive clinical monitoring in infants exposed to SSRIs *in-utero*.

There is a lack of clarity regarding the ability of SSRIs to alter ROS levels and their mechanism of action. The association between SSRIs and ROS has been reported predominantly in epidemiological and *in-vivo* studies of depression (Bilici et al., 2001; Cumurcu et al., 2009; Khanzode et al., 2003; Zafir et al., 2009). In clinical depression, the antioxidant systems are known to be inherently suppressed (Behr et al., 2012; Scapagnini et al., 2012) suggesting that the antioxidant, ROS-reducing properties of SSRIs apply only under oxidative stress (Behr et al., 2012; Dionisie et al., 2021). The reduced availability of ROS at critical timepoints during neurodevelopment may potentially interfere with known ROS-mediated signalling cascades crucial for typical neurite growth and synaptogenesis (Oswald et al., 2018). We also highlighted differences in *in-vitro* ATP levels, which we use as a surrogate marker for normal mitochondrial function. Both SH and PH have been previously shown to induce mitochondrial damage with depleted ATP levels, but in astrocytes (Then et al., 2017). Another *in-vitro* study on human placental cells also suggests that SH alters ROS and ATP levels (Nabekura et al., 2022). While our results align with some observations reported in the literature, the precise, underlying mechanisms by which SSRIs affect ROS and ATP levels remain largely unclear.

In addition to ROS and ATP levels, we detected several pathways mediated by FH, SH, and PH exposure related to energy metabolism. The SSRIs, specifically escitalopram (enantiomer of CH) and FH, have been shown to localize in cellular phospholipid membranes, cytoplasm, and endoplasmic reticulum, influencing various aspects of cellular physiology (Nichols et al., 2023). Interestingly, in human immortalised cell lines of brain origin, FH was demonstrated to activate the AMPK-ACC-CPT1 pathway (Jeon et al., 2023), which is known to play an important role in energy-related metabolic homeostasis through the regulation of mitochondrial ROS (Rabinovitch et al., 2017). FH has also been shown to enhance energy metabolism in the hippocampus of an *in-vivo* model of major depressive disorder (Filipović et al., 2022). A comprehensive multi-omics study has also supported the link between FH and increased energy metabolism across multiple rat brain regions (Rayan et al., 2022). FH exposure in mice has been shown to induce the gradual accumulation of sphingomyelin

(Gulbins et al., 2018), a pathway we highlighted in our earlier study (Arora et al., 2023) and this study. While there are fewer studies with CH, SH, and PH in this domain, CH has been known to cause *in-vitro* phospholipidosis (Hutchinson et al., 2008), and PH has been reported to cause energy metabolism changes in animal models (Park et al., 2020; Webhofer et al., 2011, 2013).

We also reported enrichments in pathways related to the metabolism of different amino acids crucial for normal brain function. In an animal model, PH demonstrated an impact on metabolites involved in amino acid metabolism (Webhofer et al., 2011). This is significant as we have previously shown differences in urinary metabolites derived from amino acids in individuals diagnosed with autism (Arora et al., 2024). Others have also reported an association of tryptophan, purine, phenylalanine, and tyrosine metabolism with autism (Boccuto et al., 2013; Dai et al., 2023; Gevi et al., 2016; Liu et al., 2019; Raghavan et al., 2022). Intriguingly, CH did not seem to have any major effects on cellular metabolism in our study despite a recent report that prenatal exposure is linked to higher rates of ADHD diagnosis (Olstad et al., 2023). We acknowledge the requirement for more work with higher doses of CH to further investigate its effects *in-vitro*.

In addition to the noteworthy enrichment of pathways, our main finding was the consistent increase of the three LPCs (LPC 16:0, LPC 18:0, and LPC 18:1) after SSRI exposures in our cellular model, followed by the clinical validation, providing a potential signpost for biomarkers of SSRI exposure and developmental outcomes. LPC 18:0 has been demonstrated to be an agonist for the peroxisome proliferator-activated receptor-gamma (PPAR-γ) pathway in a mouse model (Ma et al., 2021). In the brain, the PPAR-γ pathway has been connected with motivation and associative learning (Moosecker et al., 2021). Treatment of rodent models of autism with an agonist of the PPAR-γ pathway was shown to improve several phenotypic features (Kirsten et al., 2019; Mirza and Sharma, 2019).

We also reported a decrease in the levels of several phosphotidylcholines, which has been previously associated with autism (Qasem et al., 2017) and can be attributed to an increased activity of cytosolic phospholipase A2 (cPLA2) (Bell et al., 2004; Qasem et al., 2017). The enzyme cPLA2 hydrolyses phospholipids to LPCs and other bioactive lipids (Leslie, 2015), potentially contributing to the observed increase in LPC levels that we have reported. Further studies are required that connect cPLA2 activity upon SSRI exposure with the potential activation of the PPAR-γ pathway that could lead to premature neural differentiation (Wada et al., 2006) during early development.

We need to acknowledge that elevated LPC levels in the cord blood might not be a specific biomarker for autism and ADHD traits as there were several other metabolites associated with these outcomes in the BIS cohort (Vacy et al., 2024). However, pending further investigation, this could be more specific for *in-utero* SSRI exposure and thus related to broad number outcomes also reported in the offspring. For instance, higher levels of LPC 18:0 in maternal serum have been indicated as a biomarker for congenital heart defects (CHDs) in infants (Bahado-Singh et al., 2014). Furthermore, LPC 16:0 and LPC 18:1 levels in cord blood were positively associated with birth weight (Hellmuth et al., 2017; Lu et al., 2018; Yeum et al., 2023), a known liability factor for different cardiometabolic conditions (Lurbe and Ingelfinger, 2021). This, in turn, could be connected with PH, as its early *in-utero* exposure has been correlated with an increased liability of cardiac malformations in infants (Bérard et al., 2007, 2016). There is a link between CHDs and adverse neurodevelopmental outcomes (Latal, 2016; Marino et al., 2012), which warrants further investigation of the *in-utero* SSRI exposure effects through the LPCs. Additionally, *in-utero* SSRI exposure was found to increase anxiety and depression-related symptoms in adolescents, along with changes in the activation of fear-related brain circuitry (Zanni et al., 2025). Nevertheless, it is also essential to highlight that despite potentially adverse indicators of SSRI-mediated effects *in-utero*, a recent large-scale study demonstrated a reduction in depression-related mental health outcomes following postnatal SSRI treatment, with subsequent benefits observed on child externalising behaviours during early childhood as well (Liu et al., 2023).

Although our study has many strengths, we must also recognise its limitations. Despite employing four different cell lines, we lacked sufficient power to make strong comparisons regarding sex and/or genetic background in relation to exposure effects, indicating a need for further research. Nevertheless, we have accounted for putative genetic differences in our findings by also including cell lines derived from individuals with NDDs. While the BIS cohort provides a robust clinical validation for our *in-vitro model*, its observational design is susceptible to confounding factors, including genetic influences. Additionally, the relatively small number of infants exposed to SSRIs (n=40) limits the generalisability of our findings. We also need to acknowledge that our study did not cover the issue of SSRI withdrawal, which has been associated with neuroinflammation in a murine model and a potential elevation of ROS levels (Giatti et al., 2025). The metabolomic and neurological impact of withdrawal in early life, either at or prior to weaning, also requires evaluation. Overall, larger studies are required to determine whether LPC 16:0 and LPC 18:1 levels in cord blood statistically mediate an association between maternal SSRI use and autism-related outcomes in infants. In terms of

policy, the advantages and disadvantages of SSRI use in pregnancy requires continual revaluation as new findings, such as those described here, occur.

In conclusion, this comprehensive translational investigation provides novel insights into the metabolomic impact of prenatal SSRIs on human neuronal differentiation and neurodevelopment. We identify LPC 16:0 and LPC 18:0 as promising biomarkers of altered lipid metabolism, potentially mediating the relationship between prenatal SSRI exposure and increased likelihood of autism and ADHD traits. Future studies should clarify the molecular mechanisms underlying these metabolomic alterations and assess their clinical utility in liability prediction and targeted interventional strategies.

RESOURCE AVAILABILITY

Lead contact

Further information and requests for resources and reagents should be directed to and will be fulfilled by the lead contact, Kristiina Tammimies (kristiina.tammimies@ki.se).

Materials availability

This study did not generate any new and unique reagents.

Data and code availability

The generated data from the *in-vitro* experiments and utilised code are available on GitHub (https://github.com/Tammimies- Lab/SSRI-Metabolomics) or available upon request from the lead contact (kristiina.tammimies@ki.se). The raw data from the mass spectrometry-based metabolomics will be available on MetaboLights, upon publication. The data from the Barwon Infant Study (BIS) are available under restricted access to protect participant confidentiality. Researchers may request access by contacting the BIS Steering Committee via Anne-Louise Ponsonby at the Florey Institute of Neuroscience and Mental Health (annelouise.ponsonby@florey.edu.au). Requests are considered based on scientific and ethical considerations, and approved applications require a collaborative research agreement. Deidentified data can be shared in either Stata or CSV file formats. Further details about the cohort, data access process, and project overview are available at: www.barwoninfantstudy.org.au.

CONSORTIA

The members of the Barwon Infant Study Investigator Group are Mimi L.K. Tang, Lawrence Gray, Sarath Ranganathan, Peter Sly, Martin O'Hely, Richard Saffery, David Burgner, Len Harrison, Terry Dwyer, and John Carlin.

ACKNOWLEDGMENTS

The authors would like to thank the donors and their parents for providing valuable material for this study as a part of the RATSS (the Roots for Autism and ADHD Twin Study in Sweden) cohort. The authors acknowledge the RATSS team, especially Prof. Sven Bölte, Dr. Karl Lundin Remnelius, Dr. Johan Isaksson and Dr. Janina Neufeld for their support. The authors also acknowledge the BIS cohort participants and assistance from Lada Holland for data cleaning and verification. We thank Prof. Peter J. Meikle, Dr. Satvika Burugupalli and the Metabolomics laboratory at the Baker Institute for the conduct and advice on lipidomic lab measures for BIS. The project was supported by the Swedish Research Council (I.L., and K.T.), Swedish Foundation for Strategic Research (K.T.), the Swedish Brain Foundation – Hjärnfonden (K.T.), H.K.H. Kronprinsessan Lovisas förening för barnasjukvård och Stiftelsen Axel Tielmans minnesfond (A.A.), Strategic Research Area Neuroscience Stratneuro (K.T.), The Swedish Foundation for International Cooperation in Research and Higher Education STINT (K.T.), and Board of Research at Karolinska Institutet (K.T.). Open access funding is provided by Karolinska Institutet.

AUTHOR CONTRIBUTIONS

Conceptualization: A.A., P.V., A-L.P. and K.T.; Methodology: A.A., P.V., A-L.P. and K.T.; Software development: A.A., K. V. and K.T.; Validation: A.A., K.V., C.M., M.-O.D. F.M., J.H., X.Y. and M.O.; Formal Analysis: A.A., K.V., C.M., M.-O.D., F.M. and J.H.; Investigation: A.A., K.V., C.M., M.-O.D., F.M., J.H., X.Y. and M.O.; Resources: P.V., A-L.P., I.L. and K.T.; Data Curation: A.A., K.V., C.M. and F.M.; Writing – Original Draft: A.A., M.-O.D, J.H. and K.T.; Writing – Review & Editing: A.A. and K.T.; Visualization: A.A., K.V. and K.T.; Supervision: A-L.P., I.L., and K.T.; Project Administration: A.A. and K.T.; Funding Acquisition: A.A. and K.T.

DECLARATION OF INTERESTS

A.A., K.V, C.M., M.-O.D., F.M., J.H., X.Y., M.O., P.V., A-L.P., I.L. and K.T. declare no conflicts of interest.

SUPPLEMENTAL INFORMATION

Supplemental information can be found as an appendix to the manuscript.

REFERENCES

Ackermann, E.J., Conde-Frieboes, K., and Dennis, E.A. (1995). Inhibition of Macrophage Ca2+-independent Phospholipase A2 by Bromoenol Lactone and Trifluoromethyl Ketones. Journal of Biological Chemistry *270*, 445–450. https://doi.org/10.1074/jbc.270.1.445.

Al-abri, K., Edge, D., and Armitage, C.J. (2023). Prevalence and correlates of perinatal depression. Soc Psychiatry Psychiatr Epidemiol *58*, 1581–1590. https://doi.org/10.1007/s00127-022-02386-9.

Anderson, G.M., Czarkowski, K., Ravski, N., and Epperson, C.N. (2004). Platelet Serotonin in Newborns and Infants: Ontogeny, Heritability, and Effect of In Utero Exposure to Selective Serotonin Reuptake Inhibitors. Pediatr Res *56*, 418–422. https://doi.org/10.1203/01.PDR.0000136278.23672.A0.

Anderson, K.N., Lind, J.N., Simeone, R.M., Bobo, W.V., Mitchell, A.A., Riehle-Colarusso, T., Polen, K.N., and Reefhuis, J. (2020). Maternal Use of Specific Antidepressant Medications During Early Pregnancy and the Risk of Selected Birth Defects. JAMA Psychiatry *77*, 1246. https://doi.org/10.1001/jamapsychiatry.2020.2453.

Arora, A., Becker, M., Marques, C., Oksanen, M., Li, D., Mastropasqua, F., Watts, M.E., Arora, M., Falk, A., Daub, C.O., et al. (2023). Screening autism-associated environmental factors in differentiating human neural progenitors with fractional factorial design-based transcriptomics. Sci Rep *13*, 10519. https://doi.org/10.1038/s41598-023-37488-0.

Arora, A., Mastropasqua, F., Bölte, S., and Tammimies, K. (2024). Urine metabolomic profiles of autism and autistic traits–A twin study. PLoS ONE *19*, e0308224. https://doi.org/10.1371/journal.pone.0308224.

Bahado-Singh, R.O., Ertl, R., Mandal, R., Bjorndahl, T.C., Syngelaki, A., Han, B., Dong, E., Liu, P.B., Alpay-Savasan, Z., Wishart, D.S., et al. (2014). Metabolomic prediction of fetal congenital heart defect in the first trimester. American Journal of Obstetrics and Gynecology *211*, 240.e1-240.e14. https://doi.org/10.1016/j.ajog.2014.03.056.

Becker, M., Mastropasqua, F., Reising, J.P., Maier, S., Ho, M.-L., Rabkina, I., Li, D., Neufeld, J., Ballenberger, L., Myers, L., et al. (2020). Presynaptic dysfunction in CASK-related neurodevelopmental disorders. Transl Psychiatry *10*, 312. https://doi.org/10.1038/s41398-020-00994-0.

Behr, G.A., Moreira, J.C.F., and Frey, B.N. (2012). Preclinical and Clinical Evidence of Antioxidant Effects of Antidepressant Agents: Implications for the Pathophysiology of Major Depressive Disorder. Oxidative Medicine and Cellular Longevity *2012*, 1–13. https://doi.org/10.1155/2012/609421.

Bell, J.G., MacKinlay, E.E., Dick, J.R., MacDonald, D.J., Boyle, R.M., and Glen, A.C.A. (2004). Essential fatty acids and phospholipase A2 in autistic spectrum disorders.

Prostaglandins, Leukotrienes and Essential Fatty Acids *71*, 201–204. https://doi.org/10.1016/j.plefa.2004.03.008.

Bérard, A., Ramos, É., Rey, É., Blais, L., St.-André, M., and Oraichi, D. (2007). First trimester exposure to paroxetine and risk of cardiac malformations in infants: the importance of dosage. Birth Defect Res B *80*, 18–27. https://doi.org/10.1002/bdrb.20099.

Bérard, A., Iessa, N., Chaabane, S., Muanda, F.T., Boukhris, T., and Zhao, J.-P. (2016). The risk of major cardiac malformations associated with paroxetine use during the first trimester of pregnancy: a systematic review and meta-analysis: Paroxetine use during pregnancy increases cardiac defects in offspring. Br J Clin Pharmacol *81*, 589–604. https://doi.org/10.1111/bcp.12849.

Bilici, M., Efe, H., Köroğlu, M.A., Uydu, H.A., Bekaroğlu, M., and Değer, O. (2001). Antioxidative enzyme activities and lipid peroxidation in major depression: alterations by antidepressant treatments. Journal of Affective Disorders *64*, 43–51. https://doi.org/10.1016/S0165-0327(00)00199-3.

Boccuto, L., Chen, C.-F., Pittman, A.R., Skinner, C.D., McCartney, H.J., Jones, K., Bochner, B.R., Stevenson, R.E., and Schwartz, C.E. (2013). Decreased tryptophan metabolism in patients with autism spectrum disorders. Molecular Autism *4*, 16. https://doi.org/10.1186/2040-2392-4-16.

Bogucka, K., and Wojtczak, L. (1966). Effect of sodium azide on oxidation and phosphorylation processes in rat-liver mitochondria. Biochimica et Biophysica Acta (BBA) - Enzymology and Biological Oxidation *122*, 381–392. https://doi.org/10.1016/0926-6593(66)90031-2.

Brummelte, S., Mc Glanaghy, E., Bonnin, A., and Oberlander, T.F. (2017). Developmental changes in serotonin signaling: Implications for early brain function, behavior and adaptation. Neuroscience *342*, 212–231. https://doi.org/10.1016/j.neuroscience.2016.02.037.

Burugupalli, S., Smith, A.A.T., Oshlensky, G., Huynh, K., Giles, C., Wang, T., George, A., Paul, S., Nguyen, A., Duong, T., et al. (2022). Ontogeny of circulating lipid metabolism in pregnancy and early childhood – a longitudinal population study. eLife *11*, e72779. https://doi.org/10.7554/eLife.72779.

Chambers, S.M., Fasano, C.A., Papapetrou, E.P., Tomishima, M., Sadelain, M., and Studer, L. (2009). Highly efficient neural conversion of human ES and iPS cells by dual inhibition of SMAD signaling. Nat Biotechnol *27*, 275–280. https://doi.org/10.1038/nbt.1529.

Cinque, B., Fanini, D., Di Marzio, L., Palumbo, P., La Torre, C., Donato, V., Velardi, E., Bruscoli, S., Riccardi, C., and Cifone, M.G. (2008). Involvement of cPLA $_2$ Inhibition in Dexamethasone-Induced Thymocyte Apoptosis. Int J Immunopathol Pharmacol *21*, 539–551. https://doi.org/10.1177/039463200802100307.

Cox, J.L., Holden, J.M., and Sagovsky, R. (1987). Detection of Postnatal Depression: Development of the 10-item Edinburgh Postnatal Depression Scale. Br J Psychiatry *150*, 782–786. https://doi.org/10.1192/bjp.150.6.782.

Cumurcu, B.E., Ozyurt, H., Etikan, I., Demir, S., and Karlidag, R. (2009). Total antioxidant capacity and total oxidant status in patients with major depression: Impact of antidepressant

treatment: TAC and TOS in major depression. Psychiatry and Clinical Neurosciences *63*, 639–645. https://doi.org/10.1111/j.1440-1819.2009.02004.x.

Dai, S., Lin, J., Hou, Y., Luo, X., Shen, Y., and Ou, J. (2023). Purine signaling pathway dysfunction in autism spectrum disorders: Evidence from multiple omics data. Front. Mol. Neurosci. *16*, 1089871. https://doi.org/10.3389/fnmol.2023.1089871.

Dawson, A.L., Ailes, E.C., Gilboa, S.M., Simeone, R.M., Lind, J.N., Farr, S.L., Broussard, C.S., Reefhuis, J., Carrino, G., Biermann, J., et al. (2016). Antidepressant Prescription Claims Among Reproductive-Aged Women With Private Employer-Sponsored Insurance — United States 2008–2013. B *65*, 41–46. https://doi.org/10.15585/mmwr.mm6503a1.

De Vries, C., Gadzhanova, S., Sykes, M.J., Ward, M., and Roughead, E. (2021). A Systematic Review and Meta-Analysis Considering the Risk for Congenital Heart Defects of Antidepressant Classes and Individual Antidepressants. Drug Saf *44*, 291–312. https://doi.org/10.1007/s40264-020-01027-x.

Desaunay, P., Eude, L.-G., Dreyfus, M., Alexandre, C., Fedrizzi, S., Alexandre, J., Uguz, F., and Guénolé, F. (2023). Benefits and Risks of Antidepressant Drugs During Pregnancy: A Systematic Review of Meta-analyses. Pediatr Drugs *25*, 247–265. https://doi.org/10.1007/s40272-023-00561-2.

Dionisie, V., Ciobanu, A.M., Toma, V.A., Manea, M.C., Baldea, I., Olteanu, D., Sevastre-Berghian, A., Clichici, S., Manea, M., Riga, S., et al. (2021). Escitalopram Targets Oxidative Stress, Caspase-3, BDNF and MeCP2 in the Hippocampus and Frontal Cortex of a Rat Model of Depression Induced by Chronic Unpredictable Mild Stress. IJMS *22*, 7483. https://doi.org/10.3390/ijms22147483.

Emmerzaal, T.L., Nijkamp, G., Veldic, M., Rahman, S., Andreazza, A.C., Morava, E., Rodenburg, R.J., and Kozicz, T. (2021). Effect of neuropsychiatric medications on mitochondrial function: For better or for worse. Neuroscience & Biobehavioral Reviews *127*, 555–571. https://doi.org/10.1016/j.neubiorev.2021.05.001.

Falk, A., Koch, P., Kesavan, J., Takashima, Y., Ladewig, J., Alexander, M., Wiskow, O., Tailor, J., Trotter, M., Pollard, S., et al. (2012). Capture of neuroepithelial-like stem cells from pluripotent stem cells provides a versatile system for in vitro production of human neurons. PLoS One *7*, e29597. https://doi.org/10.1371/journal.pone.0029597.

Filipović, D., Costina, V., Findeisen, P., and Inta, D. (2022). Fluoxetine Enhances Synaptic Vesicle Trafficking and Energy Metabolism in the Hippocampus of Socially Isolated Rats. IJMS *23*, 15351. https://doi.org/10.3390/ijms232315351.

Gevi, F., Zolla, L., Gabriele, S., and Persico, A.M. (2016). Urinary metabolomics of young Italian autistic children supports abnormal tryptophan and purine metabolism. Molecular Autism *7*, 47. https://doi.org/10.1186/s13229-016-0109-5.

Giatti, S., Cioffi, L., Diviccaro, S., Chrostek, G., Piazza, R., and Melcangi, R.C. (2025). Transcriptomic Profile of the Male Rat Hypothalamus and Nucleus Accumbens After Paroxetine Treatment and Withdrawal: Possible Causes of Sexual Dysfunction. Mol Neurobiol *62*, 4935–4951. https://doi.org/10.1007/s12035-024-04592-9.

Gulbins, A., Schumacher, F., Becker, K.A., Wilker, B., Soddemann, M., Boldrin, F., Müller, C.P., Edwards, M.J., Goodman, M., Caldwell, C.C., et al. (2018). Antidepressants act by inducing autophagy controlled by sphingomyelin–ceramide. Mol Psychiatry *23*, 2324–2346. https://doi.org/10.1038/s41380-018-0090-9.

Halvorsen, A., Hesel, B., Ostergaard, S.D., and Danielsen, A.A. (2019). In Utero Exposure to SSRIs and Development of Mental Disorders: A Systematic Review and Meta-analysis. Acta Psychiatr. Scand. https://doi.org/10.1111/acps.13030.

Hellmuth, C., Uhl, O., Standl, M., Demmelmair, H., Heinrich, J., Koletzko, B., and Thiering, E. (2017). Cord Blood Metabolome Is Highly Associated with Birth Weight, but Less Predictive for Later Weight Development. Obes Facts *10*, 85–100. https://doi.org/10.1159/000453001.

Hendrick, V., Stowe, Z.N., Altshuler, L.L., Hwang, S., Lee, E., and Haynes, D. (2003). Placental Passage of Antidepressant Medications. AJP *160*, 993–996. https://doi.org/10.1176/appi.ajp.160.5.993.

Hiemke, C., and Härtter, S. (2000). Pharmacokinetics of selective serotonin reuptake inhibitors. Pharmacology & Therapeutics *85*, 11–28. https://doi.org/10.1016/S0163-7258(99)00048-0.

Hutchinson, T.H., Mahshid, Y., Jönsson, R., Björklund, C., and Kenne, K. (2008). Proteomic analysis of phospholipidosis in citalopram treated U937 cells – Support for the cholesterol biosynthesis hypothesis. Toxicology in Vitro *22*, 1198–1204. https://doi.org/10.1016/j.tiv.2008.03.016.

Jeon, S., Park, J.-E., Do, Y.H., Santos, R., Lee, S.M., Kim, B.-N., Cheong, J.H., and Kim, Y. (2023). Atomoxetine and Fluoxetine Activate AMPK-ACC-CPT1 Pathway in Human SH-SY5Y and U-87 MG Cells. Psychiatry Investig *20*, 212–219. https://doi.org/10.30773/pi.2022.0255.

Jewison, T., Su, Y., Disfany, F.M., Liang, Y., Knox, C., Maciejewski, A., Poelzer, J., Huynh, J., Zhou, Y., Arndt, D., et al. (2014). SMPDB 2.0: Big Improvements to the Small Molecule Pathway Database. Nucl. Acids Res. *42*, D478–D484. https://doi.org/10.1093/nar/gkt1067.

Josse, J., and Husson, F. (2016). missMDA: A Package for Handling Missing Values in Multivariate Data Analysis. J. Stat. Soft. *70*. https://doi.org/10.18637/jss.v070.i01.

Khanzode, S.D., Dakhale, G.N., Khanzode, S.S., Saoji, A., and Palasodkar, R. (2003). Oxidative damage and major depression: the potential antioxidant action of selective serotonin re-uptake inhibitors. Redox Report *8*, 365–370. https://doi.org/10.1179/135100003225003393.

Kirsten, T.B., Casarin, R.C., Bernardi, M.M., and Felicio, L.F. (2019). Pioglitazone abolishes cognition impairments as well as BDNF and neurotensin disturbances in a rat model of autism. Biology Open bio.041327. https://doi.org/10.1242/bio.041327.

Knudsen, T.M., Hansen, A.V., Garne, E., and Andersen, A.-M.N. (2014). Increased risk of severe congenital heart defects in offspring exposed to selective serotonin-reuptake inhibitors in early pregnancy – an epidemiological study using validated EUROCAT data. BMC Pregnancy Childbirth *14*, 333. https://doi.org/10.1186/1471-2393-14-333.

Latal, B. (2016). Neurodevelopmental Outcomes of the Child with Congenital Heart Disease. Clinics in Perinatology *43*, 173–185. https://doi.org/10.1016/j.clp.2015.11.012.

Leslie, C.C. (2015). Cytosolic phospholipase A2: physiological function and role in disease. Journal of Lipid Research *56*, 1386–1402. https://doi.org/10.1194/jlr.R057588.

Liu, A., Zhou, W., Qu, L., He, F., Wang, H., Wang, Y., Cai, C., Li, X., Zhou, W., and Wang, M. (2019). Altered Urinary Amino Acids in Children With Autism Spectrum Disorders. Front. Cell. Neurosci. *13*, 7. https://doi.org/10.3389/fncel.2019.00007.

Liu, C., Ystrom, E., and McAdams, T.A. (2023). Long-Term Maternal and Child Outcomes Following Postnatal SSRI Treatment. JAMA Netw Open *6*, e2331270. https://doi.org/10.1001/jamanetworkopen.2023.31270.

Lu, Y.-P., Reichetzeder, C., Prehn, C., Yin, L.-H., Yun, C., Zeng, S., Chu, C., Adamski, J., and Hocher, B. (2018). Cord Blood Lysophosphatidylcholine 16: 1 is Positively Associated with Birth Weight. Cell Physiol Biochem *45*, 614–624. https://doi.org/10.1159/000487118.

Lurbe, E., and Ingelfinger, J. (2021). Developmental and Early Life Origins of Cardiometabolic Risk Factors: Novel Findings and Implications. Hypertension *77*, 308–318. https://doi.org/10.1161/HYPERTENSIONAHA.120.14592.

Ma, Y., Du, X., Zhao, D., Tang, K., Wang, X., Guo, S., Li, X., Mei, S., Sun, N., Liu, J., et al. (2021). 18:0 Lyso PC, a natural product with potential PPAR-γ agonistic activity, plays hypoglycemic effect with lower liver toxicity and cardiotoxicity in db/db mice. Biochemical and Biophysical Research Communications *579*, 168–174. https://doi.org/10.1016/j.bbrc.2021.09.059.

Mansell, T., Vuillermin, P., Ponsonby, A.-L., Collier, F., Saffery, R., Barwon Infant Study Investigator Team, and Ryan, J. (2016). Maternal mental well-being during pregnancy and glucocorticoid receptor gene promoter methylation in the neonate. Dev Psychopathol *28*, 1421–1430. https://doi.org/10.1017/S0954579416000183.

Marino, B.S., Lipkin, P.H., Newburger, J.W., Peacock, G., Gerdes, M., Gaynor, J.W., Mussatto, K.A., Uzark, K., Goldberg, C.S., Johnson, W.H., et al. (2012). Neurodevelopmental Outcomes in Children With Congenital Heart Disease: Evaluation and Management: A Scientific Statement From the American Heart Association. Circulation *126*, 1143–1172. https://doi.org/10.1161/CIR.0b013e318265ee8a.

Marken, P.A. (2000). Selecting a Selective Serotonin Reuptake Inhibitor: Clinically Important Distinguishing Features. Prim Care Companion J Clin Psychiatry https://doi.org/10.4088/pcc.v02n0602.

Marques, C., Liu, L., Duncan, K.D., and Lanekoff, I. (2022). A Direct Infusion Probe for Rapid Metabolomics of Low-Volume Samples. Anal. Chem. acs.analchem.2c02918. https://doi.org/10.1021/acs.analchem.2c02918.

Mastropasqua, F., Oksanen, M., Soldini, C., Alatar, S., Arora, A., Ballarino, R., Molinari, M., Agostini, F., Poulet, A., Watts, M.E., et al. (2022). Deficiency of Heterogeneous Nuclear Ribonucleoprotein U locus leads to delayed hindbrain neurogenesis. bioRxiv 2022.09.14.507275. https://doi.org/10.1101/2022.09.14.507275.

Mirza, R., and Sharma, B. (2019). A selective peroxisome proliferator-activated receptor-γ agonist benefited propionic acid induced autism-like behavioral phenotypes in rats by attenuation of neuroinflammation and oxidative stress. Chemico-Biological Interactions *311*, 108758. https://doi.org/10.1016/j.cbi.2019.108758.

Moosecker, S., Pissioti, A., Leidmaa, E., Harb, M.R., Dioli, C., Gassen, N.C., Yu, S., Gazea, M., Catania, C., Anderzhanova, E., et al. (2021). Brain Expression, Physiological Regulation and Role in Motivation and Associative Learning of Peroxisome Proliferator-activated Receptor γ. Neuroscience *479*, 91–106. https://doi.org/10.1016/j.neuroscience.2021.10.029.

Mot, A.I., Liddell, J.R., White, A.R., and Crouch, P.J. (2016). Circumventing the Crabtree Effect: A method to induce lactate consumption and increase oxidative phosphorylation in cell culture. The International Journal of Biochemistry & Cell Biology *79*, 128–138. https://doi.org/10.1016/j.biocel.2016.08.029.

Nabekura, T., Ishikawa, S., Tanase, M., Okumura, T., and Kawasaki, T. (2022). Antidepressants induce toxicity in human placental BeWo cells. Current Research in Toxicology *3*, 100073. https://doi.org/10.1016/j.crtox.2022.100073.

Nichols, A.L., Blumenfeld, Z., Luebbert, L., Knox, H.J., Muthusamy, A.K., Marvin, J.S., Kim, C.H., Grant, S.N., Walton, D.P., Cohen, B.N., et al. (2023). Selective Serotonin Reuptake Inhibitors within Cells: Temporal Resolution in Cytoplasm, Endoplasmic Reticulum, and Membrane. J. Neurosci. *43*, 2222–2241. https://doi.org/10.1523/JNEUROSCI.1519-22.2022.

Olivier, J.D.A., Åkerud, H., Kaihola, H., Pawluski, J.L., Skalkidou, A., Högberg, U., and Sundström-Poromaa, I. (2013). The effects of maternal depression and maternal selective serotonin reuptake inhibitor exposure on offspring. Front. Cell. Neurosci. *7*. https://doi.org/10.3389/fncel.2013.00073.

Olstad, E.W., Nordeng, H.M.E., Sandve, G.K., Lyle, R., and Gervin, K. (2023). Effects of prenatal exposure to (es)citalopram and maternal depression during pregnancy on DNA methylation and child neurodevelopment. Transl Psychiatry *13*, 149. https://doi.org/10.1038/s41398-023-02441-2.

Oswald, M.C.W., Garnham, N., Sweeney, S.T., and Landgraf, M. (2018). Regulation of neuronal development and function by ROS. FEBS Lett *592*, 679–691. https://doi.org/10.1002/1873-3468.12972.

Pang, Z., Zhou, G., Ewald, J., Chang, L., Hacariz, O., Basu, N., and Xia, J. (2022). Using MetaboAnalyst 5.0 for LC–HRMS spectra processing, multi-omics integration and covariate adjustment of global metabolomics data. Nat Protoc *17*, 1735–1761. https://doi.org/10.1038/s41596-022-00710-w.

Park, D.I., Novak, B., Yan, Y., Kaya, M.E., and Turck, C.W. (2020). Paroxetine binding and activation of phosphofructokinase implicates energy metabolism in antidepressant mode of action. Journal of Psychiatric Research *129*, 8–14. https://doi.org/10.1016/j.jpsychires.2020.05.033.

Pinheiro, J.C., and Bates, D.M. (2000). Mixed-Effects Models in S and S-PLUS (New York: Springer-Verlag).

Pluskal, T., Castillo, S., Villar-Briones, A., and Orešič, M. (2010). MZmine 2: Modular framework for processing, visualizing, and analyzing mass spectrometry-based molecular profile data. BMC Bioinformatics *11*, 395. https://doi.org/10.1186/1471-2105-11-395.

Qasem, H., Al-Ayadhi, L., Al Dera, H., and El-Ansary, A. (2017). Increase of cytosolic phospholipase A2 as hydrolytic enzyme of phospholipids and autism cognitive, social and sensory dysfunction severity. Lipids Health Dis *16*, 117. https://doi.org/10.1186/s12944-016-0391-4.

R Core Team (2020). R: A language and environment for statistical computing (R Foundation for Statistical Computing, Vienna, Austria.).

Rabinovitch, R.C., Samborska, B., Faubert, B., Ma, E.H., Gravel, S.-P., Andrzejewski, S., Raissi, T.C., Pause, A., St.-Pierre, J., and Jones, R.G. (2017). AMPK Maintains Cellular Metabolic Homeostasis through Regulation of Mitochondrial Reactive Oxygen Species. Cell Reports *21*, 1–9. https://doi.org/10.1016/j.celrep.2017.09.026.

Raghavan, R., Anand, N.S., Wang, G., Hong, X., Pearson, C., Zuckerman, B., Xie, H., and Wang, X. (2022). Association between cord blood metabolites in tryptophan pathway and childhood risk of autism spectrum disorder and attention-deficit hyperactivity disorder. Transl Psychiatry *12*, 270. https://doi.org/10.1038/s41398-022-01992-0.

Rayan, N.A., Kumar, V., Aow, J., Rastegar, N., Lim, M.G.L., O'Toole, N., Aliwarga, E., Arcego, D.M., Yeo, H.T.G., Wong, J.Y., et al. (2022). Integrative multi-omics landscape of fluoxetine action across 27 brain regions reveals global increase in energy metabolism and region-specific chromatin remodelling. Mol Psychiatry *27*, 4510–4525. https://doi.org/10.1038/s41380-022-01725-1.

Risau, W., and Wolburg, H. (1990). Development of the blood-brain barrier. Trends in Neurosciences *13*. https://doi.org/10.1016/0166-2236(90)90043-A.

Rock, K.D., and Patisaul, H.B. (2018). Environmental Mechanisms of Neurodevelopmental Toxicity. Curr Envir Health Rpt *5*, 145–157. https://doi.org/10.1007/s40572-018-0185-0.

Scapagnini, G., Davinelli, S., Drago, F., De Lorenzo, A., and Oriani, G. (2012). Antioxidants as Antidepressants: Fact or Fiction? CNS Drugs *26*, 477–490. https://doi.org/10.2165/11633190-000000000-00000.

Then, C.-K., Liu, K.-H., Liao, M.-H., Chung, K.-H., Wang, J.-Y., and Shen, S.-C. (2017). Antidepressants, sertraline and paroxetine, increase calcium influx and induce mitochondrial damage-mediated apoptosis of astrocytes. Oncotarget *8*, 115490–115502. https://doi.org/10.18632/oncotarget.23302.

Tran, H., and Robb, A.S. (2015). SSRI use during pregnancy. Seminars in Perinatology *39*, 545–547. https://doi.org/10.1053/j.semperi.2015.08.010.

Uhlin, E., Rönnholm, H., Day, K., Kele, M., Tammimies, K., Bölte, S., and Falk, A. (2017). Derivation of human iPS cell lines from monozygotic twins in defined and xeno free conditions. Stem Cell Research *18*, 22–25. https://doi.org/10.1016/j.scr.2016.12.006.

Vacy, K., Thomson, S., Moore, A., Eisner, A., Tanner, S., Pham, C., Saffery, R., Mansell, T., Burgner, D., Collier, F., et al. (2024). Cord blood lipid correlation network profiles are

associated with subsequent attention-deficit/hyperactivity disorder and autism spectrum disorder symptoms at 2 years: a prospective birth cohort study. eBioMedicine *100*, 104949. https://doi.org/10.1016/j.ebiom.2023.104949.

Vanags, D.M., Larsson, P., Feltenmark, S., Jakobsson, P.-J., Orrenius, S., Claesson, H.-E., and Aguilar-Santelises, M. (1997). Inhibitors of arachidonic acid metabolism reduce DNA and nuclear fragmentation induced by TNF plus cycloheximide in U937 cells. Cell Death Differ *4*, 479–486. https://doi.org/10.1038/sj.cdd.4400269.

Vuillermin, P., Saffery, R., Allen, K.J., Carlin, J.B., Tang, M.L., Ranganathan, S., Burgner, D., Dwyer, T., Collier, F., Jachno, K., et al. (2015). Cohort Profile: The Barwon Infant Study. Int. J. Epidemiol. *44*, 1148–1160. https://doi.org/10.1093/ije/dyv026.

Wada, K., Nakajima, A., Katayama, K., Kudo, C., Shibuya, A., Kubota, N., Terauchi, Y., Tachibana, M., Miyoshi, H., Kamisaki, Y., et al. (2006). Peroxisome Proliferator-activated Receptor γ-mediated Regulation of Neural Stem Cell Proliferation and Differentiation. Journal of Biological Chemistry *281*, 12673–12681. https://doi.org/10.1074/jbc.M513786200.

Wang (2010). Selective neuronal vulnerability to oxidative stress in the brain. Fronti.Ag.Neurosci. https://doi.org/10.3389/fnagi.2010.00012.

Webhofer, C., Gormanns, P., Tolstikov, V., Zieglgänsberger, W., Sillaber, I., Holsboer, F., and Turck, C.W. (2011). Metabolite profiling of antidepressant drug action reveals novel drug targets beyond monoamine elevation. Transl Psychiatry *1*, e58–e58. https://doi.org/10.1038/tp.2011.56.

Webhofer, C., Gormanns, P., Reckow, S., Lebar, M., Maccarrone, G., Ludwig, T., Pütz, B., Asara, J.M., Holsboer, F., Sillaber, I., et al. (2013). Proteomic and metabolomic profiling reveals time-dependent changes in hippocampal metabolism upon paroxetine treatment and biomarker candidates. Journal of Psychiatric Research *47*, 289–298. https://doi.org/10.1016/j.jpsychires.2012.11.003.

Wen, X., Jeong, S., Kim, Y., Bae, J.M., Cho, N.Y., Kim, J.H., and Kang, G.H. (2017). Improved results of LINE-1 methylation analysis in formalin-fixed, paraffin-embedded tissues with the application of a heating step during the DNA extraction process. Clin Epigenet *9*, 1. https://doi.org/10.1186/s13148-016-0308-0.

Wickham, H. (2009). ggplot2 (New York, NY: Springer New York).

Yeum, D., Gilbert-Diamond, D., Doherty, B., Coker, M., Stewart, D., Kirchner, D., McRitchie, S., Sumner, S., Karagas, M.R., and Hoen, A.G. (2023). Associations of maternal plasma and umbilical cord plasma metabolomics profiles with birth anthropometric measures. Pediatr Res *94*, 135–142. https://doi.org/10.1038/s41390-022-02449-2.

Zafir, A., Ara, A., and Banu, N. (2009). In vivo antioxidant status: A putative target of antidepressant action. Progress in Neuro-Psychopharmacology and Biological Psychiatry *33*, 220–228. https://doi.org/10.1016/j.pnpbp.2008.11.010.

Zanni, G., Van Dijk, M., Cagliostro, M.C., Sepulveda, P., Pini, N., Rose, A.L., Kesin, A.L., Lugo-Candelas, C., Goncalves, P.D., MacKay, A.S., et al. (2025). Perinatal SSRI exposure impacts innate fear circuit activation and behavior in mice and humans. Nature Communications https://doi.org/10.1038/s41467-025-58785-4.

METHODS

RESOURCE TABLE

Reagent or resource	Source	Identifier
Chemicals, Peptides, and Recombinant Proteins		
Fluoxetine hydrochloride	Sigma-Aldrich	F132
Citalopram hydrobromide	Sigma-Aldrich	C7861
Sertraline hydrochloride	Sigma-Aldrich	S6319
Paroxetine hydrochloride	Sigma-Aldrich	P9623
Methanol	Sigma-Aldrich	322415
Formic Acid	Sigma-Aldrich	00940
DMEM/F-12 Glutamax	Thermo Scientific	31331-093
Glucose free DMEM	Thermo Scientific	11966025
Galactose	Sigma-Aldrich	G5388
Penicillin/ Streptomycin	Thermo Scientific	15140122
Laminin from engelbreth-holm-swarm murine cells	Sigma-Aldrich	L2020
B-27 Supplement	Thermo Scientific	17504044
N-2 Supplement	Thermo Scientific	17502001
Poly-L-ornithine	Sigma Aldrich	P3655
Recombinant human EGF	Peprotech	AF-100-15
Recombinant human bFGF	Thermo Scientific	13256-029
Bovine serum albumin	Sigma Aldrich	A7030
LPC 16:0	Sigma Aldrich	855675P
LPC 18:0	Sigma Aldrich	845875P
LPC 18:1	Sigma Aldrich	855775P
Arachidonyl trifluoromethyl ketone	Abcam	ab120350
Critical Commercial Assays		
MTS Assay	Promega	G3580
DCFDA – ROS Assay	Abcam	ab113851
Mitochondrial ToxGlo Assay	Promega	G8000

CellTiter Glow 2.0 Assay	Promega	G9242
EnzChek Phospholipase A2 Assay Kit	Invitrogen	E10217
Deposited Data		
Data and analyses source code	GitHub	github.com/Tammimies-Lab/SSRI-Metabolomics
Metabolomics raw data	MetaboLights	Available upon publication.
Software and Algorithms		
R (v4.1.2)	R	r-project.org
ggplot2 (v3.3.5)	CRAN	ggplot2.tidyverse.org
pheatmap (v1.0.12)	CRAN	cran.r-project.org/package=pheatmap
nlme (v3.1-162)	CRAN	cran.r-project.org/package=nlme
factoextra (v1.0.7)	CRAN	cran.r-project.org/package=factoextra
missMDA (v1.18)	CRAN	cran.r-project.org/package=missMDA
MetaboAnalyst 5.0	McGill University	metaboanalyst.ca
MZmine 2	OIST Japan	github.com/mzmine/mzmine2
Affinity Designer (v2.6.2)	Serif	affinity.serif.com

EXPERIMENTAL MODEL AND STUDY PARTICIPANT DETAILS

Cell culture

For the purpose of this study, previously generated and described human iPSC lines from tissue samples of a male: CTRL9II – $CTRL_{Male}$ (Uhlin et al., 2017) and female: AF22 – $CTRL_{Female}$ (Falk et al., 2012) neurotypical donors and two male donors with known genetic variants for NDDs including autism: ASD12BI – ASD_{HNRNPU} (Mastropasqua et al., 2022) and ASD17AII – ASD_{CASK} (Becker et al., 2020), were used. Information pertaining to the generation and quality control of the iPSC lines, as well as their relevant clinical background are provided in the cited publications. The iPS cells were differentiated into neural progenitor state and maintained as NES cells, as previously described (Chambers et al., 2009; Falk et al., 2012). While NES cells are neural progenitors with both neurogenic and gliogenic potential, upon differentiation they are primarily neurogenic unless they are specifically differentiated to glia (Chambers et al., 2009; Falk et al., 2012).

The NES cells were seeded (40,000 cells/cm^2) on tissue culture treated plates (Sarstedt), coated with 20 µg/mL poly-ornithine (Sigma-Aldrich) and 1 µg/mL Laminin2020 (Sigma-

Aldrich). These were grown in DMEM/F-12 Glutamax basal medium (Gibco) supplemented with 0.05x B27 (Gibco), 1x N-2 (Gibco), 10 U/ml Penicillin-Streptomycin (Gibco), 10 ng/mL recombinant human bFGF (Gibco) and 10 ng/mL recombinant human EGF (Peprotech). The undirected differentiation of NES cells to neural cell population was achieved by the withdrawal of growth factors from the culture medium (Chambers et al., 2009; Falk et al., 2012). Here, the NES cells were again seeded (40,000 cells/cm^2) on tissue culture treated plates (Sarstedt), coated with 20 µg/mL poly-ornithine (Sigma-Aldrich) and 1 µg/mL Laminin2020 (Sigma-Aldrich). However, these were grown in DMEM/F-12 Glutamax basal medium (Gibco) supplemented with 0.5x B27 (Gibco), 1x N-2 (Gibco) and 10 U/ml Penicillin-Streptomycin (Gibco). The cells were differentiated for 5 days or 28 days post induction of neural differentiation, followed by sampling based on the downstream application.

METHOD DETAILS

Selective serotonin reuptake inhibitors (SSRIs)

We evaluated the effects of fluoxetine hydrochloride (FH), citalopram hydrobromide (CH), sertraline hydrochloride (SH) and paroxetine hydrochloride (PH) in our cell lines. SSRI stock solutions of 0.01 M concentration were prepared in absolute ethanol (SH) or MilliQ H_2O (FH, CH and PH). Working solutions were prepared in MilliQ H_2O at 0.001 M. For the *in-vitro* exposures at the required concentration(s), the SSRI working solutions were subsequently mixed with DMEM/F-12 Glutamax basal medium (Gibco) supplemented with 0.5x B27 (Gibco), 1x N-2 (Gibco) and 10 U/ml Penicillin-Streptomycin (Gibco). Freshly prepared exposure medium was replaced on every second day during the period of neural differentiation.

Cytotoxicity assay

To select the appropriate treatment concentration of the SSRIs for our cell lines, we performed cytotoxicity testing. The treatment concentration ranges (0.00–30.00 µM) for the SSRIs were determined based on those optimised in our previous study using FH (Arora et al., 2023), followed by testing in the $CTRL_{Male}$ cell line using the MTS assay (Promega).

The NES cells were seeded (12,000 cells/well) in 96-well plates (Sarstedt) and exposed to a concentration range of the SSRI being evaluated. Growth factors were withdrawn from the cell culture, to initiate neural differentiation. The exposure media was changed every second day. At 24- and 120-hours (5 days) post exposure, the cells were treated with MTS (3-(4,5-dimethylthiazol-2-yl)-5-(3-carboxymethoxyphenyl)-2-(4-sulfophenyl)-2H-tetrazolium) reagent, based on instructions from the manufacturer. After 3 hours of incubation at 37˚C and

5% CO_2, absorbance was recorded at 490 nm using a spectrophotometric microplate reader (FLUOstar Omega, BMG Labtech).

Quantification of percentage viability at each concentration and timepoint was done in R (v4.1.2) (R Core Team, 2020). The response was represented as a regression line generated using the Loess method for local regression fitting, and the shaded area denoted the 95% confidence interval. Two-way ANOVA, followed by Tukey's post-hoc correction for multiple comparisons, was used to test for significance (adj. $p<0.05$) of the reported findings.

Cellular ROS assay

The cellular ROS assay (Abcam) was used to determine total ROS levels at day 5 and 28 of SSRI exposures (FH, CH and PH: 3.0 µM; SH: 1.5 µM). In short, NES cells were seeded (12,000 cells/well) in dark walled, clear bottom 96-well plates (Sarstedt) and allowed to adhere overnight at 37°C, 5% CO_2 incubation. Thereafter, neural differentiation was induced by withdrawing growth factors from the culture medium accompanied by exposure to the SSRIs, with the culture medium being changed on every alternative day.

The culture medium was aspirated, and the cells were exposed to the fluorogenic dye, DCFDA (2',7'-dichlorodihydrofluorescein diacetate), at a concentration of 10 µM, in 100 µL of 1X Buffer (from the kit) and incubated at 37°C, 5% CO_2 for 45 minutes. Fluorescence at excitation wavelength 485 nm and emission wavelength 520 nm was recorded using a spectrophotometric microplate reader (FLUOstar Omega, BMG Labtech). All readings were reported as percentage of control. Normality testing was performed using the Shapiro-Wilk Test. Subsequently, Kruskal-Wallis rank sum test, followed by Nemenyi's post-hoc correction for multiple comparisons, was used to test for the significance (adj. $p<0.05$) of the reported findings in R (v4.1.2) (R Core Team, 2020).

Mitochondrial ToxGlo assay

To test and correct for the Crabtree effect (Mot et al., 2016), the mitochondrial ToxGlo assay (Promega) was used to check for mitochondrial vulnerability, with effects on oxidative phosphorylation and subsequent ATP generation, to the potent mitotoxin sodium azide (Bogucka and Wojtczak, 1966). In short, NES cells were seeded (12,000 cells/well) in white walled, clear bottom 96-well plates (Greiner) and allowed to adhere overnight at 37°C, 5% CO_2 incubation. The assay was used to determine cell membrane integrity and adenosine triphosphate (ATP) levels after 24 hours, in accordance with the optimised manufacturer's instructions (Promega).

On the next day, the culture medium was replaced with glucose free DMEM (Gibco) supplemented with 10 mM galactose (Sigma-Aldrich), instead of DMEM-F12 Glutamax basal medium (Gibco), 90 minutes prior to the assay. The galactose induced the cells to primarily rely on oxidative phosphorylation to produce ATP, instead of glycolysis. Cell membrane integrity was assessed by measuring a distinct protease activity associated with necrosis using a fluorogenic peptide substrate, bis-AAF-R110. After incubation at 37°C, 5% CO_2 for 30 minutes, fluorescence at excitation wavelength 485 nm and emission wavelength 520 nm was recorded using a spectrophotometric microplate reader (FLUOstar Omega, BMG Labtech).

Next, the ATP detection reagent was added, causing cell lysis, and producing a luminescent signal proportional to the amount of total ATP present. Immediately after, luminescence was recorded using a spectrophotometric microplate reader (FLUOstar Omega, BMG Labtech). All readings were reported as percentage of control. Two-way ANOVA followed by Tukey's post-hoc correction for multiple comparisons, was used to test for significance (adj. $p<0.05$) of the reported findings in R (v4.1.2) (R Core Team, 2020).

Cellular ATP assay

The CellTiter Glow 2.0 assay (Promega) was used to quantify the total ATP levels generated by oxidative phosphorylation in response to the SSRI exposures. This was done at day 5 (FH, CH and PH: 3.0 µM; SH: 1.5 µM) and day 28 of SSRI exposures (FH, CH, SH and PH: 1.5 µM). In short, NES cells were seeded (12,000 cells/well) in white walled, clear bottom 96-well plates (Greiner) and allowed to adhere overnight at 37°C, 5% CO_2 incubation. Thereafter, neural differentiation was induced by withdrawing growth factors from the culture medium and exposure to SSRIs, with the culture medium being changed at every alternative day.

On day 5 and day 28 post induction of neural differentiation, the culture medium (100 µL/well) was replaced with glucose free DMEM (Gibco) supplemented with 10 mM galactose, instead of DMEM-F12 Glutamax basal medium (Gibco), 90 minutes prior to the assay. Thereafter, the cells were incubated at room temperature for 30 minutes followed by the addition of the CellTiter Glo 2.0 reagent (100µL/well) and mixing on an orbital shaker for 2 minutes to induce cell lysis. The cells were then incubated at room temperature for another 10 minutes followed by recording luminescence using a spectrophotometric microplate reader (FLUOstar Omega, BMG Labtech).

All readings were reported as percentage of control. For the day 5 results, normality testing was performed using the Shapiro-Wilk Test. Subsequently, Two-way ANOVA followed by Tukey's post-hoc correction for multiple comparisons, was used to test for

significance (adj. $p<0.05$) of the reported findings. For the day 28 results, normality testing was also performed using the Shapiro-Wilk Test. Subsequently, the Dunn (1964) Kruskal-Wallis multiple comparison with p-values adjusted with the Holm method was used to test for significance (adj. $p<0.05$) of the reported findings in R (v4.1.2) (R Core Team, 2020).

Direct infusion electrospray ionisation mass spectrometry (ESI-MS)

Untargeted metabolomic profiling was performed using the direct infusion probe (DIP) for ESI-MS (Marques et al., 2022) on snap-frozen cells at day 5 (N=120) and day 28 (N=120) of SSRI exposures during neural differentiation of NES cells, with two biological replicates having three technical replicates each for the treated and untreated groups in all four cell lines: $CTRL_{Male}$, $CTRL_{Female}$, ASD_{HNRNPU} and ASD_{CASK}. For the day 5 samples, the cells were exposed to 3.0 µM of FH, CH and PH, and 1.5 µM of SH, as per the previously determined concentrations based on the cytotoxicity assays (Figure S1A). For the day 28 samples, the cells were exposed to a standardised dose of 1.5 µM to enable direct comparison of long-term exposure related metabolomic effects induced by each SSRI.

The cell culture plates were stored at -80˚C prior to lysing with the electrospray solvent containing 9:1 methanol:water, with 0.1% formic acid and 28 internal standards. To enable comparisons, all cell samples were normalized to total cell counts per sample. The samples were analysed on a QExactive™ Orbitrap instrument (Thermo Scientific) at mass resolving power of 140,000 ($m/\Delta m$) using untargeted full scanning between 70 and 1000 Da in positive mode. The resulting data was extracted using 30 seconds data per sample and sorted in MZmine 2 (Pluskal et al., 2010). One-point quantification of metabolite concentrations in the sample was calculated using the intensity ratio of endogenous metabolite to the internal standard and multiplied with the concentration of the internal standard (Marques et al., 2022).

Differential metabolomics and feature selection

Principal component analysis (PCA) was performed in R (v4.1.2) (R Core Team, 2020) followed by visualisation with the *factoextra* package (v1.0.7) (https://cran.r-project.org/package=factoextra). Prior to the PCA, any missing values (0.03% of the dataset) were imputed using the *missMDA* package (v1.18) (Josse and Husson, 2016) in R (v4.1.2) (R Core Team, 2020). Here, the number of dimensions of the PCA were estimated by cross-validation using the k-fold method followed by imputation of missing values using the PCA model.

To test for significance of the resulting metabolite concentrations (µM) following the mass spectrometry analysis workflow, a mixed linear model using the *nlme* package (v3.1-162) (Pinheiro and Bates, 2000) in R (v4.1.2) (R Core Team, 2020) was applied to the dataset for each SSRI (FH, CH, SH and PH) at each timepoint (day 5, day 28). Any missing values were treated as *NA* values. Here, the mixed linear model used was *lme(concentration ~ exposure, random = ~ 1 | cell line)*. The data was filtered prior to the application of the mixed linear model, based on the SSRI exposure. The obtained p values were adjusted for multiple comparisons using the FDR method in R (v4.1.2) (R Core Team, 2020). Significantly modulated metabolites (Treatment vs. Control) were selected based on a significance threshold of adjusted $p<0.05$ and were visualised using the *ggplot2* package (v3.3.5) (Wickham, 2009) in R (v4.1.2) (R Core Team, 2020).

Feature selection of shared SSRI effects on the metabolites was performed using the statistical meta-analysis module of MetaboAnalyst 5.0 (Pang et al., 2022). Metabolite concentration lists were provided for each SSRI at day 5 and day 28, respectively. Followed by performing an automated data integrity check, normalisation was performed using log2 transformation and data-scaling. Data scaling adjusts each variable/feature by a scaling factor computed based on the dispersion of the variable, in this case auto-scaling was used (mean-centred and divided by the standard deviation of each variable). For the selection of significant features that were shared by all exposure conditions, p values from each analysis were combined using the Fisher's method, $-2*\sum\text{Log}(p)$. A combined *T statistic* and combined p value was provided for each metabolite (feature), which were used for selecting significant shared features (combined $p<0.05$).

Pathway enrichment analysis

Detected metabolites were tested for enrichment in the Small Molecule Pathway Database (SMPDB) (Jewison et al., 2014) using the quantitative enrichment analysis (QEA) approach to metabolite set enrichment analysis (MSEA) from the enrichment analysis module of MetaboAnalyst 5.0 (Pang et al., 2022). Any missing values were imputed using the in-built K-Nearest Neighbour (KNN) algorithm for similar samples. The metabolite labels of 172 out of 189 metabolites were successfully mapped to PubChem (https://pubchem.ncbi.nlm.nih.gov) and annotated with PubChem CIDs. The remainder (17) were excluded from the analysis. The concentration data was normalised using data-scaling (auto-scaling, as done in the feature selection). The cut-off threshold for entries from metabolite sets to be included from the metabolite set library was set to 2.

QEA uses a generalised linear model to estimate a *Q-statistic* for each metabolite set, which describes the correlation between compound concentration profiles, X, and clinical outcomes, Y. The *Q statistic* for a metabolite set is the average of the *Q statistics* for each metabolite in the set. The cut-off threshold for entries from metabolite sets to be included was set to 2. Based on the statistical testing, enrichment dot-plots and pathway networks were generated. In the pathway networks, 2 or more nodes were only connected by an edge when the number of shared metabolites was >25% of the combined metabolites contributing to each node.

Lipid exposure and cPLA2 inhibition

Solutions of the selected LPCs (16:0, 18:0 and 18:1) were prepared in methanol (stock: 0.01 M) and used immediately by warming up at 37°C or stored at -20°C for future use. Working solutions were prepared based on the determined concentration of the LPCs at day 5 of SH exposure (LPC 16:0 – 2.0 µM, LPC 18:0 – 1.8 µM and LPC 18:1 – 0.8 µM), from the mass spectrometry based-metabolomics (Figure 3A). The cells were exposed to a 2X:mixture of the LPCs at the initiation of undirected differentiation and every media change (alternative feeding days). LPC synthesis was inhibited by tandemly exposing the differentiating cells with 10.0 µM $AACOCF_3$ (arachidonyl trifluoromethyl ketone), a known phospholipase-A2 (PLA2) inhibitor (Ackermann et al., 1995; Cinque et al., 2008; Vanags et al., 1997). Cellular ROS and cellular ATP assays were performed at day 5 and 28 of exposure, as described in the previous sections. All readings were reported as percentage of control. Two-way ANOVA followed by Tukey's post-hoc correction for multiple comparisons, was used to test for significance (adj. $p<0.05$) of the reported findings in R (v4.1.2) (R Core Team, 2020).

Population-based mother-child cohort

The Barwon Infant Study (BIS) consists of 1074 mother-child pairs (including 10 sets of twins) recruited from the Barwon region (Victoria, Australia) recruited antenatally between July 2010 and July 2013. Cohort details, including population characteristics, eligibility and exclusion criteria, and data collection methods, have been described elsewhere (Vuillermin et al., 2015).

Information on antidepressant use, including the type used, was collected in a medication questionnaire during the 28-week antenatal review (1st and 2nd trimester). In addition, the Edinburgh Post Natal Depression Scale (EPDS) (Cox et al., 1987) was administered during the 28-week antenatal review. This is a widely used and validated measure

of depression that assesses mood over a one-week period. Further details are described earlier (Mansell et al., 2016).

Lipidomic measures were obtained from cord blood serum sample (obtained from the umbilical cord blood at birth, then placed into serum clotting tubes and analysed with ultra-high-performance-tandem mass spectrometry (UHPLC-MS/MS). The time from blood collection to processing and storage, as well as the total duration of storage at -80°C, was recorded and considered in the subsequent analysis. Maternal blood contamination in cord blood samples was assessed using DNA methylation profiling based on previously established methods (Vacy et al., 2024; Wen et al., 2017).

The details of the UHPLC-MS/MS analysis are described elsewhere (Burugupalli et al., 2022). Briefly, 776 lipid features were quantified, including LPC 16:0, LPC 18:0, and LPC 18:1, with the fatty acyl moiety at either the sn1 or sn2 position. These were chosen *a priori* based on the results of the *in-vitro* experiments. Lipids were extracted using a 1:1 butanol solution with 10 mM ammonium formate, which included a mixture of internal standards. The analysis was conducted using UHPLC-MS/MS on an Agilent 6490 QQQ mass spectrometer coupled with an Agilent 1290 series UHPLC system. Separation was achieved using two ZORBAX Eclipse Plus C18 columns (21 × 100 mm, 18 mm, Agilent) at a temperature of 45°C. Mass spectrometry was performed in both positive and negative ion modes with dynamic scheduled multiple reaction monitoring. Lipid species concentrations were determined by comparing them to the corresponding internal standards. Further details, data processing and quantification have been described previously (Burugupalli et al., 2022; Vacy et al., 2024).

ADHD and autism-related symptoms were assessed using the Child Behaviour Checklist for ages 1.5–5 (CBCL) at 2 years and the Strengths and Difficulties Questionnaire P4-10 (SDQ) at 4 years, methods described elsewhere (Vacy et al., 2024). Specifically, the DSM-5-oriented subscales for attention-deficit/hyperactivity problems (CBCL-ADHP) and autism spectrum problems (CBCL-ASP) from the CBCL were utilised, along with the SDQ subscales for hyperactivity (SDQ-hyper), peer problems (SDQ-peer), and prosocial behaviour (SDQ-prosocial). The questionnaires were completed by the child's parent or guardian.

Multivariate regression models were applied to assess the association between prenatal SSRI use, antidepressant use, and EBDS score and LPC levels in cord blood. Multivariate regression models, with LPCs split into categories based on quartiles, to allow for nonlinear associations with dose-response and neurodevelopmental outcomes, were also assessed. Covariates included child sex, gestational age, time sample spent on the bench and in the freezer before analysis, contamination of the child's blood with maternal blood, and child's

birth weight. LPC-neurodevelopmental outcomes were additionally adjusted at the child's age the CBCL or SDQ was completed. Nominal statistical significance was considered at $p<0.05$ and trends at $p<0.10$.

QUANTIFICATION AND STATISTICAL ANALYSIS

All statistical analyses were performed in R (v4.1.2) (R Core Team, 2020). The statistical models and tests used for the analyses are described in the methodology relevant to the experimental technique, in the sections above. All plots, unless otherwise stated, were created using the *ggplot2* package (v3.3.5) (Wickham, 2009) or the *pheatmap* package (v1.0.12, https://CRAN.R-project.org/package=pheatmap) in R (v4.1.2) (R Core Team, 2020).

FIGURE LEGENDS

Main figures

Figure 1. In-vitro assays and differential metabolomics following selective serotonin reuptake inhibitor (SSRI) exposure in differentiating neuroepithelial stem cells. A. *In-vitro* assay determined total ROS levels at day 5 and day 28 of fluoxetine (FH), citalopram (CH), sertraline (SH) and paroxetine (PH) exposure (adjusted p: *<0.05, **<0.01, ***<0.001). **B.** *In-vitro* assay determined total ATP levels at day 5 and day 28 of fluoxetine (FH), citalopram (CH), sertraline (SH) and paroxetine (PH) exposure (adjusted p: *<0.05, **<0.01, ***<0.001). **C.** Distribution of significant metabolites across metabolite classes at day 5 and day 28. **D.** Heatmap of estimate values from the applied mixed linear model for metabolites and SSRIs, with a significant overlap across at least two SSRIs (adjusted p: a<0.05, b<0.01, c<0.001).

Figure 2. Enrichment of detected metabolites detected in biochemical pathways. A. Enrichment dot-plot of top 10 significantly enriched metabolic pathways (adjusted $p \leq 0.05$) following fluoxetine (FH), sertraline (SH) and paroxetine (PH) exposure at day 5 and day 28. **B.** Interaction network of top 50 enriched metabolic pathways following sertraline (SH) exposure at day 28. **C.** Interaction network of top 50 enriched metabolic pathways following paroxetine (PH) exposure at day 28.

Figure 3. Association of selected LPCs with SSRI exposures and neurodevelopmental disorder outcome measures. A. Detected concentration of selected LPCs following *in-vitro* SSRI exposure at day 5 and 28 (adjusted p: *<0.05, **<0.01,

***<0.001). **B.** *In-vitro* assay determined total ROS levels at day 5 and day 28 of LPC inhibition (adjusted p: *<0.05, **<0.01, ***<0.001). **C.** *In-vitro* assay determined total ATP levels at day 5 and day 28 of LPC inhibition (adjusted p *<0.05, **<0.01, ***<0.001). **D.** Adjusted estimated mean change in doubling of LPC concentration (with 95% confidence interval, CI), per exposure. **E.** Adjusted estimated mean change in CBCL (Child Behaviour Checklist) Autism Spectrum Problems and CBCL Attention Deficit Hyperactivity Problems (with 95% CI) by quartiles of LPC concentrations (Q1, reference group).

Supplementary figures

Figure S1. Cellular assays for method optimisations. **A.** Cell viability at 24 hours and 120 hours (day 5) of fluoxetine (FH; from Arora et al., 2023), citalopram (CH), sertraline (SH) and paroxetine (PH) exposure using the MTS assay. **B.** Optimisation of the shift from glycolysis to oxidative phosphorylation using glucose free, galactose supplemented medium and testing with sodium azide exposure using a mitotoxicity assay (cell membrane permeability and total ATP). **C.** Detection of FH, CH, SH, and PH in the mass spectrometry readout following *in-vitro* exposure at day 5 and 28.

Figure S2. Analysis of selective serotonin reuptake inhibitor (SSRI) exposure effects. **A.** PCA scatter plot of detected metabolites following fluoxetine (FH), citalopram (CH), sertraline (SH) and paroxetine (PH) exposure at day 5. **B.** PCA scatter plot of detected metabolites following fluoxetine (FH), citalopram (CH), sertraline (SH) and paroxetine (PH) exposure at day 28. **C.** Interaction network of top 50 enriched metabolic pathways following sertraline (SH) exposure at day 5. **C.** Interaction network of top 50 enriched metabolic pathways following paroxetine (PH) exposure at day 5. **E.** *In-vitro* assay determined total ROS levels at day 5 and day 28 of LPC inhibition (adjusted p: *<0.05, **<0.01, ***<0.001). **F.** *In-vitro* assay determined total ATP levels at day 5 and day 28 of LPC inhibition (adjusted p *<0.05, **<0.01, ***<0.001).

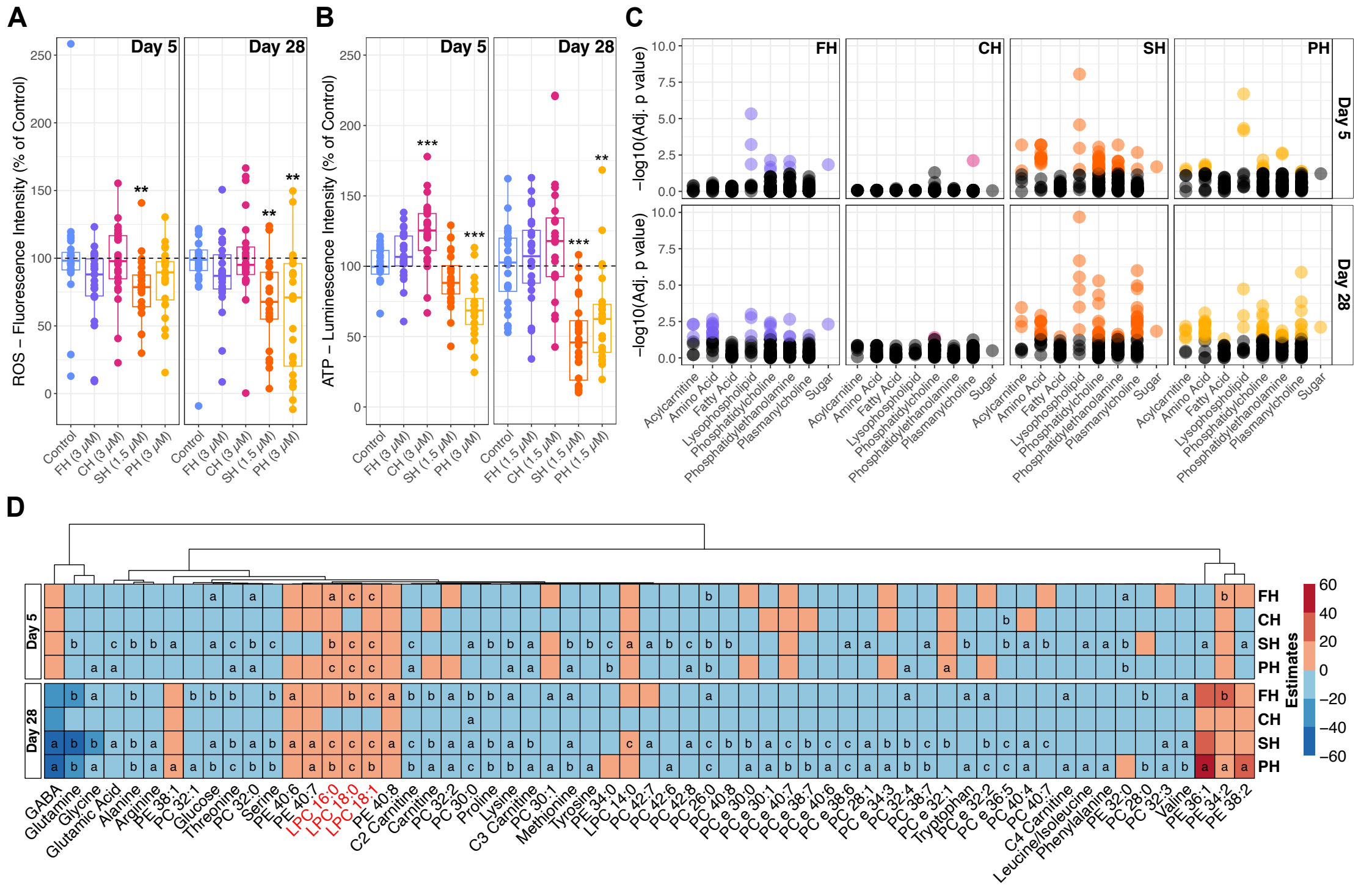
A
Day 5
Day 28
ROS – Fluorescence Intensity (% of Control)
Control
FH (3 μM)
CH (3 μM)
SH (1.5 μM)
PH (3 μM)
B
ATP – Luminescence Intensity (% of Control)
FH (1.5 μM)
CH (1.5 μM)
PH (1.5 μM)
C
FH
CH
SH
PH
−log10(Adj. p value)
Acylcarnitine
Amino Acid
Fatty Acid
Lysophospholipid
Phosphatidylcholine
Phosphatidylethanolamine
Plasmanylcholine
Sugar
D
Estimates
GABA
Glutamine
Glycine
Glutamic Acid
Alanine
Arginine
PE 38:1
PC 32:1
Glucose
Threonine
PC 32:0
Serine
PE 40:6
PE 40:7
LPC 16:0
LPC 18:0
LPC 18:1
PE 40:8
C2 Carnitine
Carnitine
PC 32:2
PC 30:0
Proline
Lysine
C3 Carnitine
PC 30:1
Methionine
Tyrosine
PE 34:0
LPC 14:0
PC 42:7
PC 42:6
PC 42:8
PC 26:0
PC 40:8
PC e 30:0
PC e 30:1
PC e 40:7
PC e 38:7
PC e 40:6
PC e 38:6
PC 28:1
PC e 34:3
PC 32:4
PC 38:7
PC e 32:1
Tryptophan
PC e 32:2
PC e 36:5
PC 40:4
PC 40:7
C4 Carnitine
Leucine/Isoleucine
Phenylalanine
PE 32:0
PC 28:0
PC 32:3
Valine
PE 36:1
PE 34:2
PE 38:2

Figure 1

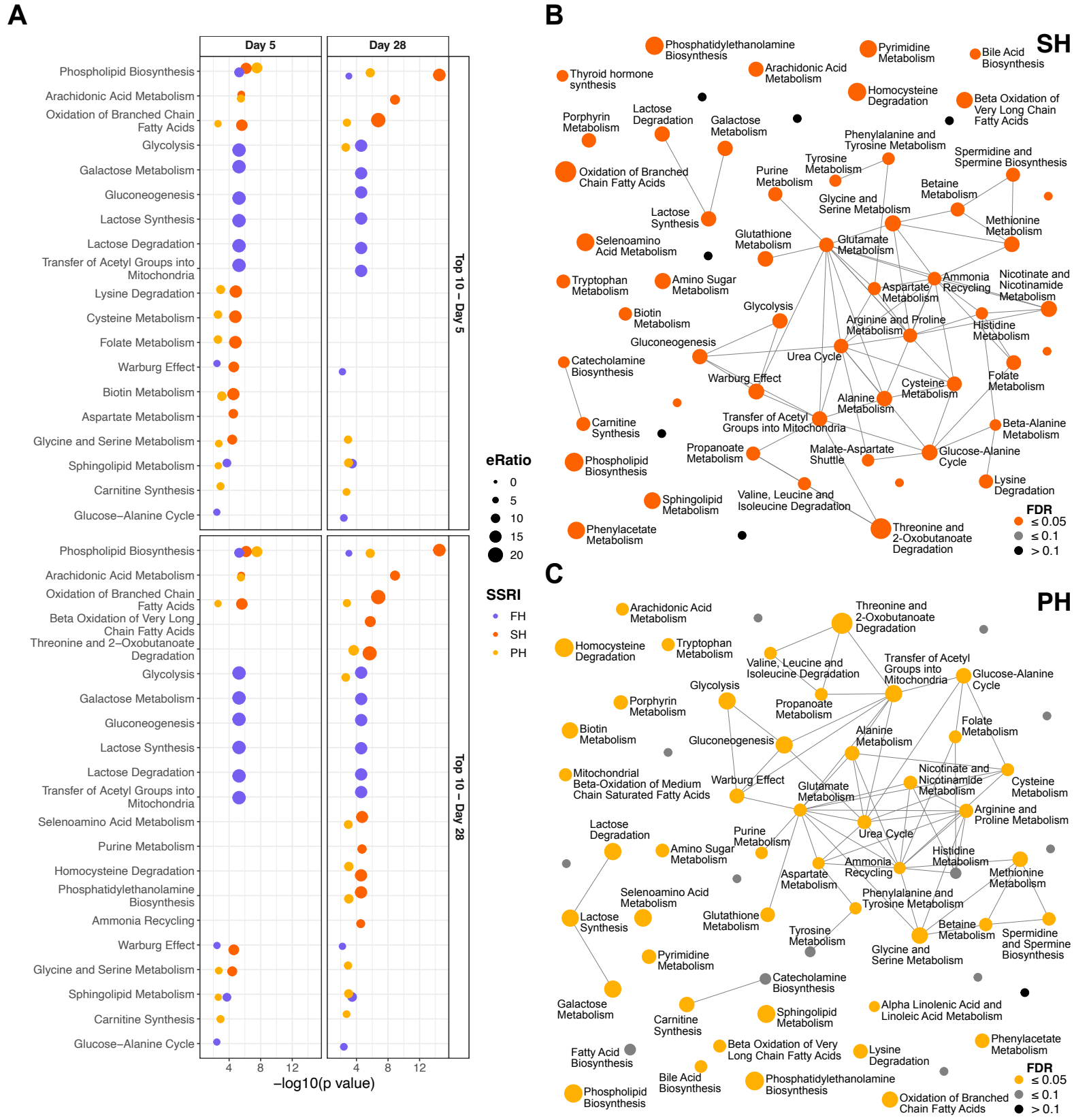
A
Day 5
Day 28
Phospholipid Biosynthesis
Arachidonic Acid Metabolism
Oxidation of Branched Chain Fatty Acids
Glycolysis
Galactose Metabolism
Gluconeogenesis
Lactose Synthesis
Lactose Degradation
Transfer of Acetyl Groups into Mitochondria
Lysine Degradation
Cysteine Metabolism
Folate Metabolism
Warburg Effect
Biotin Metabolism
Aspartate Metabolism
Glycine and Serine Metabolism
Sphingolipid Metabolism
Carnitine Synthesis
Glucose–Alanine Cycle
Top 10 – Day 5
Beta Oxidation of Very Long Chain Fatty Acids
Threonine and 2–Oxobutanoate Degradation
Selenoamino Acid Metabolism
Purine Metabolism
Homocysteine Degradation
Phosphatidylethanolamine Biosynthesis
Ammonia Recycling
Top 10 – Day 28
4
8
12
–log10(p value)
eRatio
0
5
10
15
20
SSRI
FH
SH
PH
B
SH
Phosphatidylethanolamine Biosynthesis
Pyrimidine Metabolism
Bile Acid Biosynthesis
Thyroid hormone synthesis
Arachidonic Acid Metabolism
Homocysteine Degradation
Beta Oxidation of Very Long Chain Fatty Acids
Porphyrin Metabolism
Lactose Degradation
Galactose Metabolism
Phenylalanine and Tyrosine Metabolism
Spermidine and Spermine Biosynthesis
Oxidation of Branched Chain Fatty Acids
Tyrosine Metabolism
Purine Metabolism
Betaine Metabolism
Glycine and Serine Metabolism
Lactose Synthesis
Methionine Metabolism
Selenoamino Acid Metabolism
Glutathione Metabolism
Glutamate Metabolism
Tryptophan Metabolism
Amino Sugar Metabolism
Ammonia Recycling
Nicotinate and Nicotinamide Metabolism
Aspartate Metabolism
Biotin Metabolism
Glycolysis
Arginine and Proline Metabolism
Histidine Metabolism
Gluconeogenesis
Urea Cycle
Catecholamine Biosynthesis
Folate Metabolism
Warburg Effect
Cysteine Metabolism
Alanine Metabolism
Carnitine Synthesis
Transfer of Acetyl Groups into Mitochondria
Beta-Alanine Metabolism
Propanoate Metabolism
Malate-Aspartate Shuttle
Glucose-Alanine Cycle
Phospholipid Biosynthesis
Lysine Degradation
Sphingolipid Metabolism
Valine, Leucine and Isoleucine Degradation
Phenylacetate Metabolism
Threonine and 2-Oxobutanoate Degradation
FDR
≤ 0.05
≤ 0.1
> 0.1
C
PH
Arachidonic Acid Metabolism
Threonine and 2-Oxobutanoate Degradation
Homocysteine Degradation
Tryptophan Metabolism
Valine, Leucine and Isoleucine Degradation
Transfer of Acetyl Groups into Mitochondria
Glucose-Alanine Cycle
Glycolysis
Porphyrin Metabolism
Propanoate Metabolism
Biotin Metabolism
Folate Metabolism
Gluconeogenesis
Alanine Metabolism
Mitochondrial Beta-Oxidation of Medium Chain Saturated Fatty Acids
Warburg Effect
Nicotinate and Nicotinamide Metabolism
Cysteine Metabolism
Glutamate Metabolism
Arginine and Proline Metabolism
Lactose Degradation
Purine Metabolism
Urea Cycle
Amino Sugar Metabolism
Histidine Metabolism
Ammonia Recycling
Methionine Metabolism
Aspartate Metabolism
Selenoamino Acid Metabolism
Phenylalanine and Tyrosine Metabolism
Lactose Synthesis
Glutathione Metabolism
Betaine Metabolism
Tyrosine Metabolism
Spermidine and Spermine Biosynthesis
Glycine and Serine Metabolism
Pyrimidine Metabolism
Catecholamine Biosynthesis
Galactose Metabolism
Alpha Linolenic Acid and Linoleic Acid Metabolism
Carnitine Synthesis
Sphingolipid Metabolism
Phenylacetate Metabolism
Beta Oxidation of Very Long Chain Fatty Acids
Fatty Acid Biosynthesis
Lysine Degradation
Bile Acid Biosynthesis
Phosphatidylethanolamine Biosynthesis
Phospholipid Biosynthesis
Oxidation of Branched Chain Fatty Acids
FDR
≤ 0.05
≤ 0.1
> 0.1

Figure 2

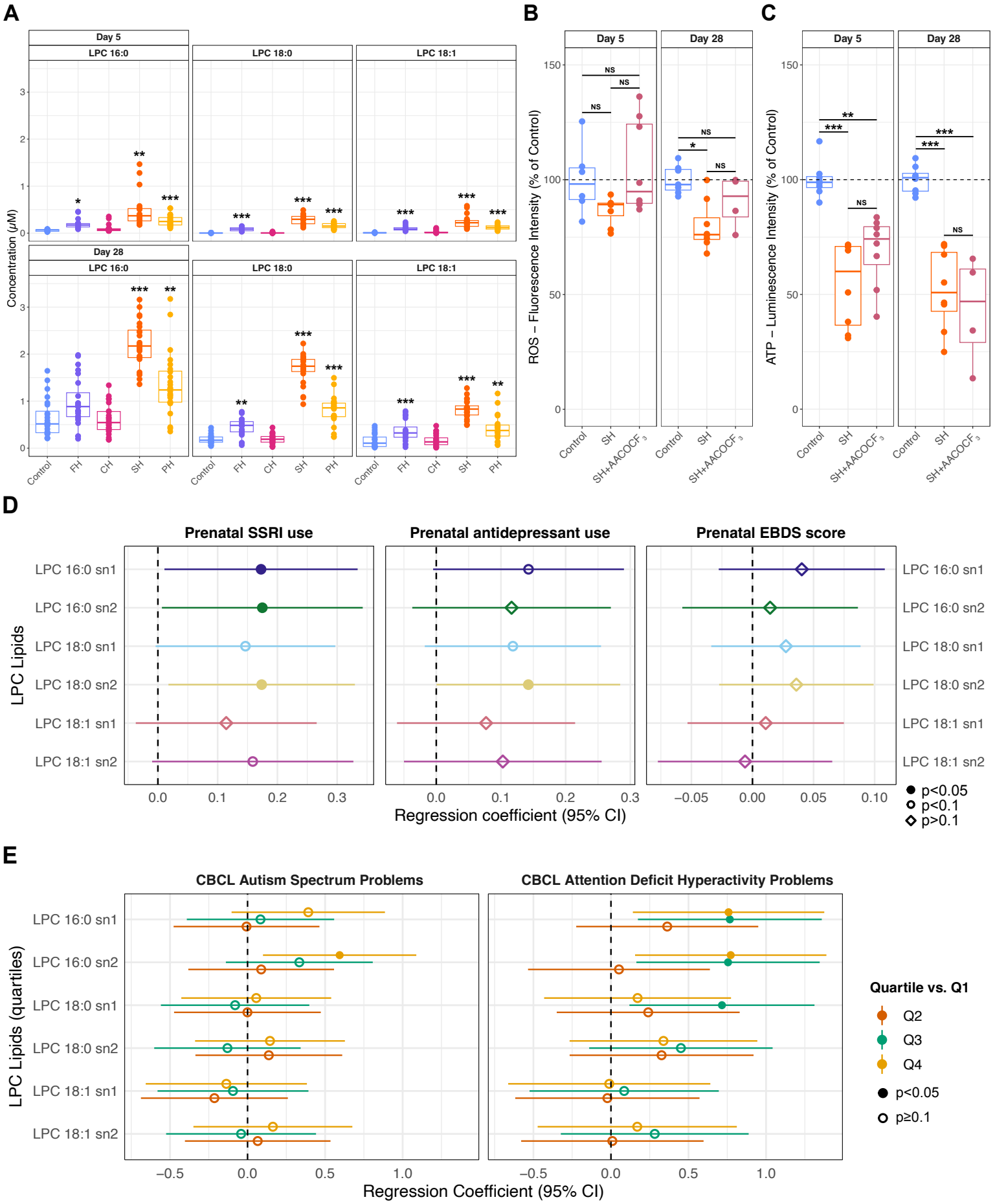
A
Day 5
LPC 16:0
LPC 18:0
LPC 18:1
Day 28
Concentration (μM)
Control
FH
CH
SH
PH
B
Day 5
Day 28
ROS – Fluorescence Intensity (% of Control)
NS
SH+AACOCF3
C
ATP – Luminescence Intensity (% of Control)
D
Prenatal SSRI use
Prenatal antidepressant use
Prenatal EBDS score
LPC Lipids
LPC 16:0 sn1
LPC 16:0 sn2
LPC 18:0 sn1
LPC 18:0 sn2
LPC 18:1 sn1
LPC 18:1 sn2
Regression coefficient (95% CI)
p<0.05
p<0.1
p>0.1
E
CBCL Autism Spectrum Problems
CBCL Attention Deficit Hyperactivity Problems
LPC Lipids (quartiles)
Regression Coefficient (95% CI)
Quartile vs. Q1
Q2
Q3
Q4
p<0.05
p≥0.1

Figure 3

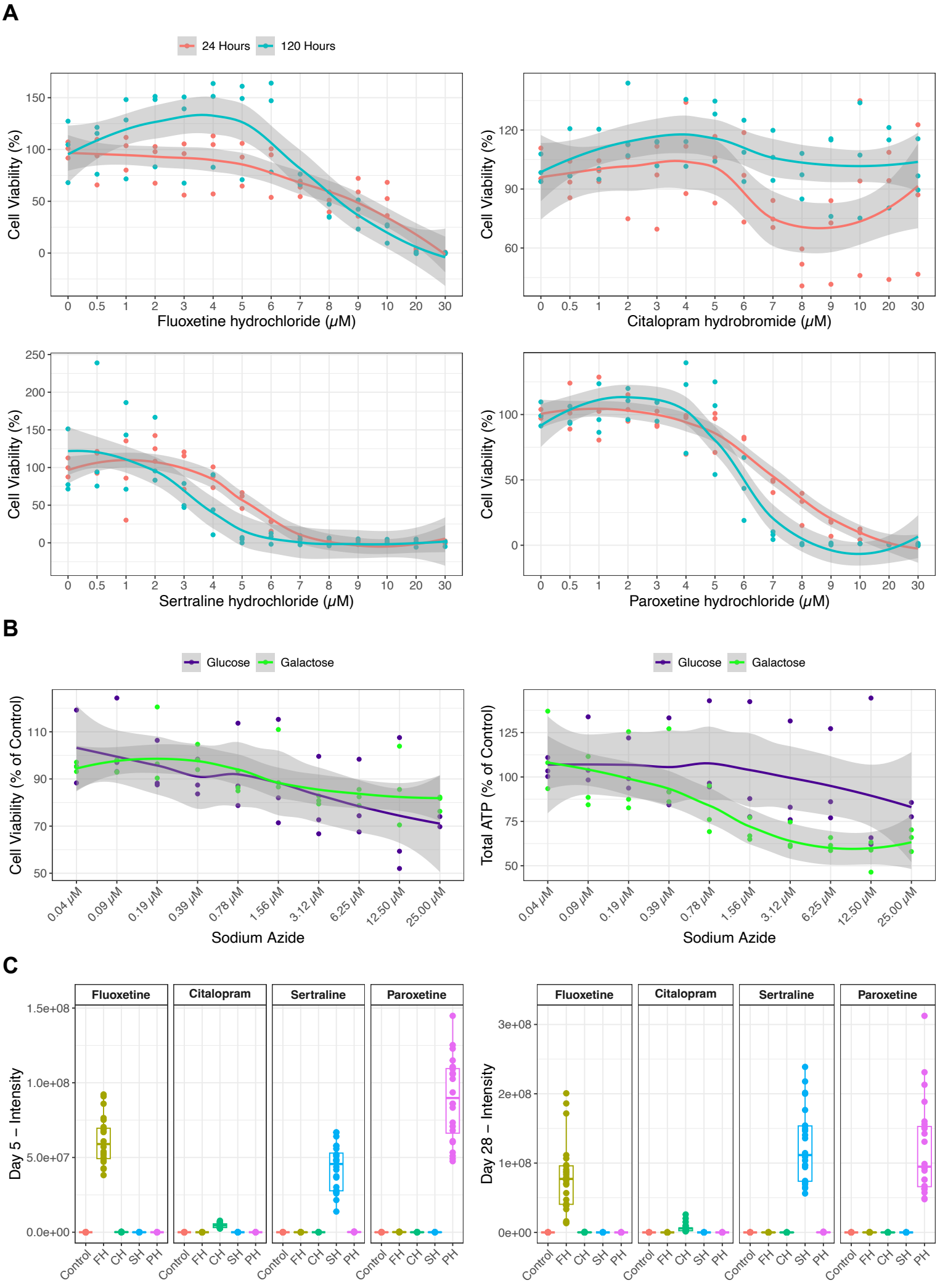
A
24 Hours
120 Hours
Cell Viability (%)
Fluoxetine hydrochloride (μM)
Citalopram hydrobromide (μM)
Sertraline hydrochloride (μM)
Paroxetine hydrochloride (μM)
B
Glucose
Galactose
Cell Viability (% of Control)
Total ATP (% of Control)
Sodium Azide
0.04 μM
0.09 μM
0.19 μM
0.39 μM
0.78 μM
1.56 μM
3.12 μM
6.25 μM
12.50 μM
25.00 μM
C
Fluoxetine
Citalopram
Sertraline
Paroxetine
Day 5 – Intensity
Day 28 – Intensity
Control
FH
CH
SH
PH

Figure S1

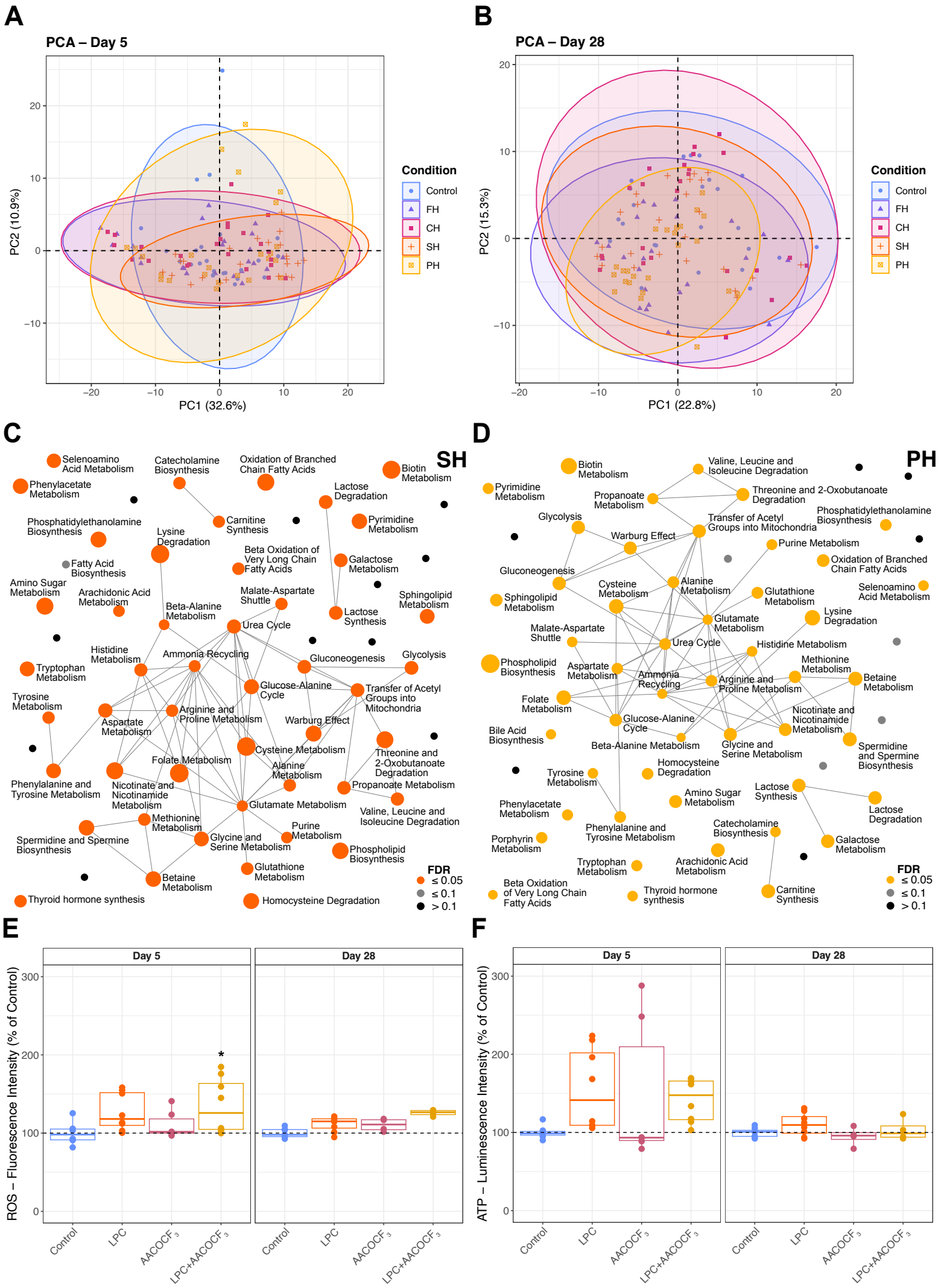
A
PCA – Day 5
PC2 (10.9%)
PC1 (32.6%)
Condition
Control
FH
CH
SH
PH
B
PCA – Day 28
PC2 (15.3%)
PC1 (22.8%)
Condition
Control
FH
CH
SH
PH
C
SH
Selenoamino Acid Metabolism
Catecholamine Biosynthesis
Oxidation of Branched Chain Fatty Acids
Biotin Metabolism
Phenylacetate Metabolism
Lactose Degradation
Phosphatidylethanolamine Biosynthesis
Carnitine Synthesis
Pyrimidine Metabolism
Lysine Degradation
Beta Oxidation of Very Long Chain Fatty Acids
Fatty Acid Biosynthesis
Galactose Metabolism
Amino Sugar Metabolism
Arachidonic Acid Metabolism
Malate-Aspartate Shuttle
Sphingolipid Metabolism
Beta-Alanine Metabolism
Lactose Synthesis
Urea Cycle
Histidine Metabolism
Ammonia Recycling
Gluconeogenesis
Glycolysis
Tryptophan Metabolism
Glucose-Alanine Cycle
Transfer of Acetyl Groups into Mitochondria
Tyrosine Metabolism
Arginine and Proline Metabolism
Aspartate Metabolism
Warburg Effect
Cysteine Metabolism
Threonine and 2-Oxobutanoate Degradation
Folate Metabolism
Alanine Metabolism
Phenylalanine and Tyrosine Metabolism
Nicotinate and Nicotinamide Metabolism
Propanoate Metabolism
Glutamate Metabolism
Valine, Leucine and Isoleucine Degradation
Methionine Metabolism
Purine Metabolism
Spermidine and Spermine Biosynthesis
Glycine and Serine Metabolism
Phospholipid Biosynthesis
Glutathione Metabolism
Betaine Metabolism
Thyroid hormone synthesis
Homocysteine Degradation
FDR
≤ 0.05
≤ 0.1
> 0.1
D
PH
Biotin Metabolism
Valine, Leucine and Isoleucine Degradation
Pyrimidine Metabolism
Propanoate Metabolism
Threonine and 2-Oxobutanoate Degradation
Phosphatidylethanolamine Biosynthesis
Glycolysis
Transfer of Acetyl Groups into Mitochondria
Warburg Effect
Purine Metabolism
Oxidation of Branched Chain Fatty Acids
Gluconeogenesis
Cysteine Metabolism
Alanine Metabolism
Selenoamino Acid Metabolism
Glutathione Metabolism
Sphingolipid Metabolism
Lysine Degradation
Glutamate Metabolism
Malate-Aspartate Shuttle
Urea Cycle
Histidine Metabolism
Phospholipid Biosynthesis
Methionine Metabolism
Aspartate Metabolism
Ammonia Recycling
Arginine and Proline Metabolism
Betaine Metabolism
Folate Metabolism
Nicotinate and Nicotinamide Metabolism
Glucose-Alanine Cycle
Bile Acid Biosynthesis
Beta-Alanine Metabolism
Glycine and Serine Metabolism
Spermidine and Spermine Biosynthesis
Homocysteine Degradation
Tyrosine Metabolism
Lactose Synthesis
Amino Sugar Metabolism
Lactose Degradation
Phenylacetate Metabolism
Phenylalanine and Tyrosine Metabolism
Catecholamine Biosynthesis
Porphyrin Metabolism
Galactose Metabolism
Tryptophan Metabolism
Arachidonic Acid Metabolism
Beta Oxidation of Very Long Chain Fatty Acids
Thyroid hormone synthesis
Carnitine Synthesis
FDR
≤ 0.05
≤ 0.1
> 0.1
E
Day 5
Day 28
ROS – Fluorescence Intensity (% of Control)
Control
LPC
AACOCF3
LPC+AACOCF3
F
Day 5
Day 28
ATP – Luminescence Intensity (% of Control)
Control
LPC
AACOCF3
LPC+AACOCF3

Figure S2